



**NTNU – Trondheim**  
Norwegian University of  
Science and Technology

# Fabrication and characterisation of a vertically aligned Forest of Carbon Nanotubes towards a superhydrophobic Surface

**Jon-Oddvar Kolnes**

Nanotechnology

Submission date: June 2015

Supervisor: Zhiliang Zhang, KT

Co-supervisor: Jianying He, KT

Norwegian University of Science and Technology  
Department of Structural Engineering



## Abstract

Owing to their unique water repellent properties, superhydrophobic surfaces offer a vast number of potential industrial applications. From self-cleaning windows to more efficient microfluidic devices, research on what makes a surface repel water has led to several energy-saving solutions.

This thesis investigates the possibility that a surface of vertically aligned carbon nanotubes (CNTs) can be made superhydrophobic by functionalisation with perfluorododecyltrichlorosilane (FDTS). The characteristics that govern wetting behaviour and makes a surface water repellent are reviewed, with particular focus on the importance of contact angles and the water adhesion force. The unique properties of carbon nanotubes are presented, and methods for growth and fabrication of CNT surfaces are summarised.

By the use of plasma enhanced chemical vapour deposition (PECVD), a carbon nanotube surface is grown on a silicon substrate. A barrier layer of aluminium oxide separates the substrate from the iron catalyst on which carbon growth is initiated. The surface is examined by the use of scanning electron microscopy (SEM) and transmission electron microscopy (TEM), revealing the grown CNTs to be multi-walled CNTs (MWCNTs), with lengths of  $5\ \mu\text{m}$  and tube widths ranging from 8 nm to 50 nm. To achieve superhydrophobicity, the structure is treated by oxygen plasma and a solution of FDTS that lowers the surface energy. Contact angles are measured, and recorded to be as high as  $130^\circ$ . By using a tensiometer, water adhesion forces were measured, with the lowest observed value value being  $279.3\ \mu\text{N}$ .

Those are typical characteristics of a hydrophobic surface. Although not superhydrophobic, both surface structure and functionalisation show an impressive improvement compared to the original unstructured substrate.



## Sammendrag

Superhydrofobiske overflater kan, på grunn av deres unike vannavstøtende egenskaper, by på en rekke mulige industrielle anvendelser. Alt i fra selvrensende vinduer til mer effektive mikrofluidiske innretninger, forskning på hva som får en overflate til å frastøte vann har ført til flere energisparende løsninger.

Denne avhandlingen utforsker mulighetene for at en overflate av oppstilte karbonnanorør kan gjøres superhydrofobisk gjennom funksjonalisering med perfluordodekyltriklorosilan (FDTS). De karakteristiske preg som styrer overflatefuktning gjennomgås, med særskilt fokus på viktigheten av kontaktvinkler og vannadhesjonskrefter. De unike særpregne til karbonnanorør, i tillegg til metoder for vekst og fremstilling av karbon nanorøroverflater blir presentert.

En karbonnanorøroverflate er blitt fremstilt på silisiumssubstrat ved å bruke plasma forbedret kjemisk dampavsetning (PECVD). Aluminiumoksid ble deponert som barrierelag for å hindre diffusjon mellom substrat og det katalytiske jernlaget hvor karbonvekst blir initiert. Den ferdige overflaten undersøkes ved bruk av sveipeelektronmikroskopi (SEM) og transmisjonselektronmikroskopi (TEM). Dette åpenbarer ferdigstilte flerveggede karbonnanorør (MWCNT), med lengder på rundt 5  $\mu\text{m}$  og diametere som strekker seg fra 8 nm til 50 nm. For å oppnå superhydrofobisitet behandles strukturen med oksygenplasma og en løsning av FDTS som senker overflateenergien. Kontaktvinkler måles og 130° registreres som høyeste observerte verdi. Ved hjelp av en strekkmåler kan adhesjonskrefter mellom vann og overflate måles, og laveste verdi registreres til 279.3  $\mu\text{m}$ .

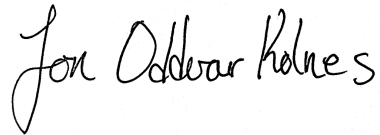
Disse verdiene er karakteristiske for en hydrofobisk overflate. Selv om det ikke kvalifiserer til en superhydrofobisk betegnelse, så viser både overflatestruktur og funksjonalisering til en imponerende forbedring sammenlignet med den originale, ustrukturerte flaten.



## **Preface**

This master's thesis is the culmination of my efforts during the spring semester of 2015, thus concluding my five years master's degree programme in Nanotechnology at the Norwegian University of Science and Technology (NTNU). The work has been carried out at the NTNU Nanomechanical Lab at the Department of Structural Engineering, and the NTNU Nanolab. It is also part of a larger collaborative project between the NTNU Nanomechanical Lab and Statoil ASA.

Trondheim, June 22, 2015

A handwritten signature in black ink, reading "Jon Oddvar Kolnes". The signature is written in a cursive style with a large initial 'J'.

Jon Oddvar Kolnes





## **Acknowledgment**

I would like to thank my supervisors, Associate Professor Jianying He and Professor Zhiliang Zhang at the Department of Structural Engineering at NTNU, for their great interest, and excellent guidance during my thesis work. Your advice has always been appreciated and I am very grateful for your support. A great thank you also to PhD candidate Zhiwei He for performing contact angle measurements, and for superb help in developing and perfecting the experimental method. I would also like to thank PhD candidate Mao Wang who provided great help with water adhesion measurements.

The acquisition and processing of TEM images could not have been accomplished without the great help of Aleksander B. Mosberg who took time out of his own thesis writing to assist me.

Thank you to NTNU Nanolab senior engineer Espen Rogstad for his great technical support with regards to the necessary instruments and processes of the NTNU Nanolab, in particular the ever unreliable PECVD. The Research Council of Norway is acknowledged for the support to NTNU NanoLab through the Norwegian Micro- and Nano-Fabrication Facility, NorFab (197411/V30).

J.O.K.



# Contents

Abstract . . . . .	iii
Sammendrag . . . . .	v
Preface . . . . .	vii
Acknowledgment . . . . .	ix
<b>List of Acronyms</b>	<b>xiii</b>
<b>1 Introduction</b>	<b>1</b>
1.1 Background . . . . .	1
1.2 Purpose of the thesis . . . . .	2
1.3 Outline of the Thesis . . . . .	3
<b>2 Wetting and Water-Repellency</b>	<b>5</b>
2.1 Contact Angles . . . . .	6
2.2 Water Adhesion . . . . .	11
2.3 Superhydrophobic Surfaces . . . . .	13
<b>3 Carbon Nanotubes</b>	<b>17</b>
3.1 Fabrication of Carbon Nanotubes . . . . .	17
3.2 Growth of Carbon Nanotubes . . . . .	20
<b>4 Experimental Method</b>	<b>25</b>
4.1 Fabricating the samples . . . . .	25
4.2 Characterisation . . . . .	28
4.3 Testing . . . . .	29

<b>5 Results and Discussion</b>	<b>33</b>
5.1 Characterisation . . . . .	33
5.2 Water Repellency . . . . .	41
<b>6 Conclusion and Outlook</b>	<b>49</b>
6.1 Conclusion . . . . .	49
6.2 Outlook and Further Work . . . . .	50
<b>Bibliography</b>	<b>53</b>
<b>Appendices</b>	<b>65</b>
<b>A TEM Results</b>	<b>67</b>
<b>B Water Adhesion Results</b>	<b>69</b>

# List of Acronyms

**AFM** Atomic Force Microscope

**CA** Contact Angle

**CNF** Carbon Nanofiber

**CNT** Carbon Nanotube

**CVD** Chemical Vapour Deposition

**DCAT** Dynamic Contact Angle Measuring Instrument and Tensiometer

**EDX** Energy Dispersive X-ray Spectroscopy

**FDTS** Perfluorododecyltrichlorosilane

**MWCNT** Multi Wall Carbon Nanotube

**NPD** Norwegian Petroleum Directorate

**NCS** Norwegian Continental Shelf

**PDMS** Polydimethylsiloxane

**PECVD** Plasma Enhanced Chemical Vapour Deposition

**PTFE** Polytetrafluorethylene

**S(T)EM** Scanning (Transmission) Electron Microscope

**SWCNT** Single Wall Carbon Nanotube



# Chapter 1

## Introduction

### 1.1 Background

The Johan Castberg field is located in the Barents Sea, nearly 250 km north of the Norwegian main land. Three oil discoveries (the earliest one from 2011) form the resource base for the field, and oil volume estimates make it one of the largest licenses in the Barents Sea. Following the first discoveries, interest in the Barents Sea increased, leading to several other successful explorations. Lundin Norway AS recently made a significant oil and gas discovery, while Statoil ASA, the operator of the Johan Castberg field, share interest in licenses even further north where oil also has been proved.<sup>1-5</sup>

In 2013, a study by the Norwegian Petroleum Directorate (NPD) estimated that about 42 % of all undiscovered recoverable oil and gas resources on the Norwegian continental shelf (NCS) is located in the Barents Sea area.<sup>6</sup> An increase in exploration activities in this area is therefore to be expected in decades to come.

However, the northern, Arctic climate poses serious difficulties regarding the further development of industrial activities. A recent study by North Energy ASA selected several possible challenges due to the extreme weather conditions that must be considered. In addition to temperatures as low as  $-40^{\circ}\text{C}$ , snowfalls, winds and polar lows, issues due to icing is a heavy concern.<sup>7</sup> The study further states that “Icing as a result of sea spray and atmospheric ice, Polar lows, Arctic storms and

troughs, combined with high waves and 24-hour darkness for about two to three months, will create very demanding working conditions". With operations moving farther north, icing must be considered a safety threat.

There is a range of methods for dealing with ice. They can be described as either active de-icing methods or passive anti-icing methods.<sup>8</sup> De-icing methods involves the removal of ice using external thermal heat, mechanical energy, high-velocity fluids or other active energy-demanding methods. While these alternatives can be effective in removing ice, they are often costly and energy-consuming, as they require a continuous application when ice has already built up. Anti-icing methods try to avoid ice accretion altogether, and are thus a great passive solution.<sup>9</sup> Even though there is no known material that completely avoids build-up of ice, some water repellent coatings provide reduced adhesion and therefore offer great potential.<sup>10</sup>

What makes a surface icephobic is thought to be related to how water droplets behaves on water repellent surfaces, also called hydrophobic- or superhydrophobic surfaces. Such surfaces have shown both reduced ice adhesion, and delayed freezing time.<sup>11-15</sup> These surfaces are designed so that the contact area between the solid substrate and liquid droplet will be as small as possible. This is done by increasing the roughness of the surface, usually by creating a micro/nanoscale hierarchical structures. This structure will then introduce pockets of air in the surface that suspend the droplet, so that the droplet is more easily repelled. If such a surface is also covered in a hydrophobic coating that repels water molecules, the surface should show superhydrophobic behaviour.

A structure made up of carbon nanotubes (CNTs) has great potential use in a superhydrophobic surface. Due to the high ratio between length and diameter of a single tube, a surface covered in CNTs will experience a massive increase in active surface area. When this area is made hydrophobic by a coating, air will get trapped between the CNT protrusions and the surface is predicted to show exceptional water repellent properties.

## **1.2 Purpose of the thesis**

This thesis will detail some of the aspects that make a surface water repellent, and how they can be utilised in the design of a superhydrophobic surface. Carbon nanotubes (CNTs) are introduced, and the most common methods for growth and fab-



rication are outlined. With particular focus on the fabrication through the use of plasma enhanced chemical vapour deposition (PECVD), an experimental method for the fabrication of a vertically aligned CNT surface is developed. The finalised structure is made hydrophobic through functionalisation with oxygen plasma and FDTS. The CNT structure is examined through the use of scanning electron microscopy (SEM) and transmission electron microscopy (TEM). Through a measure of contact angles and water adhesive forces, the water repellent properties of the surface are tested and evaluated.

### **1.3 Outline of the Thesis**

- Chapter 2 presents how functionalisation and surface structure are related to wetting states. The chapter also reveals how contact angles and water adhesive forces can be used as evidence of hydrophobicity.
- Chapter 3 reviews the most common methods of fabricating carbon nanotubes, with particular focus on the use of PECVD. The details of the CNT growth mechanism is also presented.
- Chapter 4 lays out the experimental method that has been used in this work. It includes not only the fabrication design of a sample, but also methods for structural characterisation, and examination of water repellent properties.
- Chapter 5 examines the results gained from the method in the previous chapter.
- Chapter 6 summarises the most important results in this thesis, with focus on some particular areas for future consideration.
- Appendix contains remaining results that were not detailed in chapter 5.



## Chapter 2

# Wetting and Water-Repellency

The fascinating self-cleaning property of water droplets rolling down a lotus leaf has for many years made people wonder about the true nature of water repellent surfaces. In addition to the lotus leaf, other biological organisms with unique wettability properties have been observed. This includes the water strider with its exceptional water-walking abilities, the mosquito with the antifogging properties of its eyes, the water repellent cuticle of the springtail, and many other intriguing designs.<sup>16-24</sup>

Many of these properties found in nature offer a great potential in industrial applications. That is why scientists aim to study and replicate these characteristics through biomimetic research, which inspires design from nature. The development of the scanning electron microscope (SEM), and other high resolution electron microscopes, has allowed the close investigation of these special surface structures. Structures that usually are composed of micro- and nano-scaled building blocks, as can be seen from the SEM-images in figures 2.1 and 2.2. Adapting these designs in technological application have allowed the creation of self-cleaning windows, materials with enhanced corrosion resistance, in addition to various anti-sticking and anti-icing surfaces.<sup>22</sup>

For a quantitative analysis of wetting behaviour, one can consider two simple methods. For a resting droplet, the contact angle (CA) between droplet and surface, and the force of adhesion between water and surface both provide a means of determining the water repellent properties of a surface.

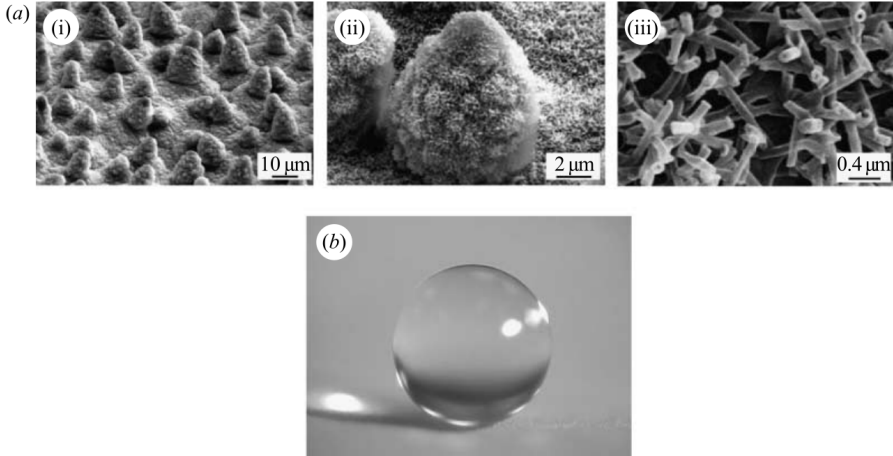


**Figure 2.1:** (a) SEM images of the lotus leaf surface, at three magnifications. (b) Image of a single water droplet resting on the lotus leaf.<sup>25</sup>

## 2.1 Contact Angles

### Flat Surface

For a single liquid droplet resting on a flat, smooth solid surface, a CA can be measured along the contact line between droplet and surface as indicated by figure 2.3. The wettability can be expressed by this angle, and is given by Young's equation:

$$\cos \theta = \frac{\gamma_{SV} - \gamma_{SL}}{\gamma_{LV}}. \quad (2.1)$$

Here,  $\theta$  is the contact angle at equilibrium, while  $\gamma_{SV}$ ,  $\gamma_{SL}$  and  $\gamma_{LV}$  denote the interfacial surface tensions between the respective phases (S = solid, V = vapour, and L = liquid) at the triple point line.

The equilibrium at the triple point line decides the CA and thus also the wetting nature of the surface. A CA of less than  $5^\circ$  results in a high degree of wetting, making it a superhydrophilic surface. Less than  $90^\circ$  denotes a hydrophilic surface and higher than  $90^\circ$  is a hydrophobic surface. For surfaces with very little wetting, a contact angle larger than  $150^\circ$  can be observed, this is considered a superhydrophobic

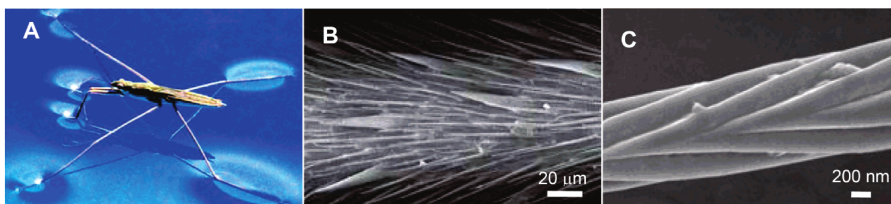


**Figure 2.2:** (a) A water strider resting gently on the water surface. (b) SEM image of the leg of a water strider covered in micro-sized, needle-shaped hairs. (c) SEM image of a single hair, showing nano-sized grooves.<sup>18</sup>

surface.<sup>27</sup> A schematic representation can be viewed in figure 2.4.

A flat, smooth surface can be made hydrophobic by covering the surface in a layer of water-repellent coating. These coatings are usually based on fluorine-terminated organic compounds.<sup>28</sup> Fluorine is very effective for chemical lowering of the surface free energy because of its small atomic radius and high electronegativity.<sup>29</sup> Examples include polytetrafluoroethylene (PTFE) and perfluorododecyltrichlorosilane (FDTS) who both have proven to give high contact angles and low surface free energy.  $-\text{CH}_x$  groups do also have quite a low surface energy,<sup>30</sup> thus coatings without fluorine end-groups have also successfully been used, including acetone and polydimethylsiloxane.<sup>31–40</sup>

The CA on a flat surface of PTFE is typically  $\sim 115\text{--}120^\circ$ . Higher CAs than this can generally not be accomplished on a flat surface alone. Increasing the surface roughness is therefore necessary to gain superhydrophobicity.<sup>28</sup>

## Rough Surface

The superhydrophobic phenomena is usually a result of a rough or structured area caused by micro- and nano-asperities. Two models have been developed to explain how the apparent CA changes when surface roughness is introduced. The models considers the situation where the droplet either penetrates the asperities (Wenzel model), or where it is suspended on top of them (Cassie-Baxter model) as seen in figure 2.5.

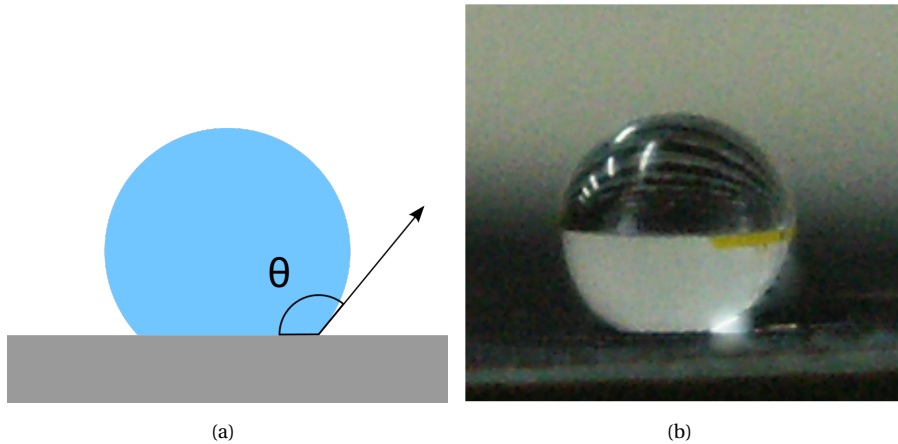


**Figure 2.3:** (a) Behaviour of a liquid droplet on a flat, solid surface. Contact angle measured at the contact line. (b) A liquid water droplet placed on a pigeon feather.<sup>26</sup>

### Wenzel model

Robert N. Wenzel suggested that the purpose of a roughened surface was to magnify the wetting properties of a solid. That way, a solid substance with a positive wetting tendency would wet more readily, the rougher the surface. A smooth water-repelling surface would repel more when roughened.<sup>41</sup> He argued that this was because of the larger contact area between the liquid and the surface, and introduced a roughness factor  $r$ :

$$r = \text{roughness factor} = \frac{\text{actual surface}}{\text{geometric surface}},$$

which he then introduced into equation (2.1):

$$\cos \theta' = \frac{r(\gamma_{sv} - \gamma_{sl})}{\gamma_{lv}}. \quad (2.2)$$

$\theta'$  is then the contact angle on the rough surface, with the interfacial surface tensions remaining the same. The relationship between the two equations (2.1) and (2.2) is then given by:

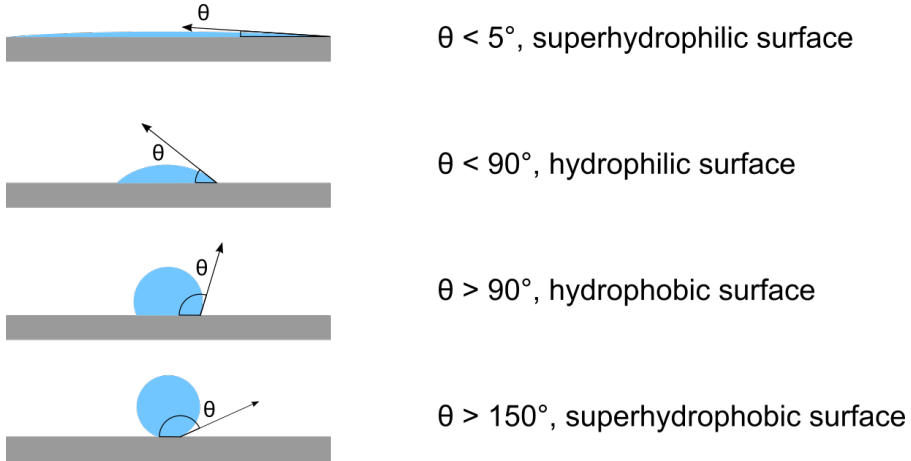


**Figure 2.4:** Schematic representation of a water droplet on a superhydrophilic, hydrophilic, hydrophobic and superhydrophobic surface.

$$\cos\theta' = r \cos\theta. \quad (2.3)$$

Equation 2.3 then clearly indicates that a surface with a higher roughness factor will in fact become more water-repellent if the initial CA  $\theta$  is higher than  $90^\circ$  and vice versa for a wetting surface. The dependence of the CA on the roughness factor is presented in figure 2.6.

### Cassie-Baxter model

For a non-wetting surface with a high roughness factor, the droplet might not actually penetrate the asperities, giving the situation in figure 2.5(b), and described by the Cassie-Baxter model.<sup>42</sup> In this case, the droplet is not only in contact with the surface structure, but also pockets of air, and this composite solid-liquid-air interface requires a different approach. To determine the CA for such a surface,  $\phi_s$  represents the fraction of the solid substrate in contact with the liquid droplet, and the equation is then given as:<sup>43</sup>

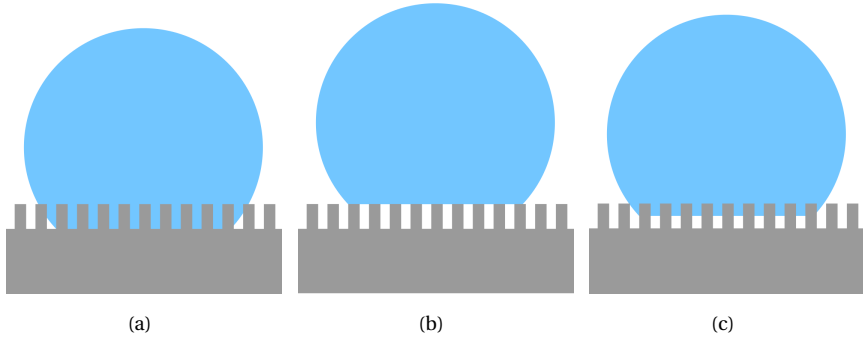


**Figure 2.5:** Schematic illustration of a water droplet resting on a surface in the (a) Wenzel state, in the (b) Cassie-Baxter state and in a (c) mixed state.

$$\cos \theta' = \phi_S (\cos \theta + 1) - 1 \quad (2.4)$$

Therefore, for a superhydrophobic surface, the contribution of the solid part should be as small as possible.

Depending on the surface characteristics, a mixed, interstitial state can also be observed, one in which the asperities are only partially penetrated. These models offer a useful approach of describing the wetting state of a water droplet resting on a surface. However, it should be noted that the equations proposed by Wenzel and Cassie-Baxter are not entirely correct as they argue that the CA is determined by the contact area between the droplet and surface. Recent studies have shown that the CA is a result of the three-phase structure at the contact line.<sup>44–46</sup> Figure 2.7 shows how changing both the topography and the chemical nature of the surface beneath the droplet would not change the CA as long as the contact line remained the same.

Nevertheless, the models offer valuable insight into the different wetting states, and the equations can be used to prove transitions from one wetting state to another. In most practical cases, the equations still work quite well, owing to the fact that the contact line experience the same surface topography as that found under the droplet.<sup>27</sup>



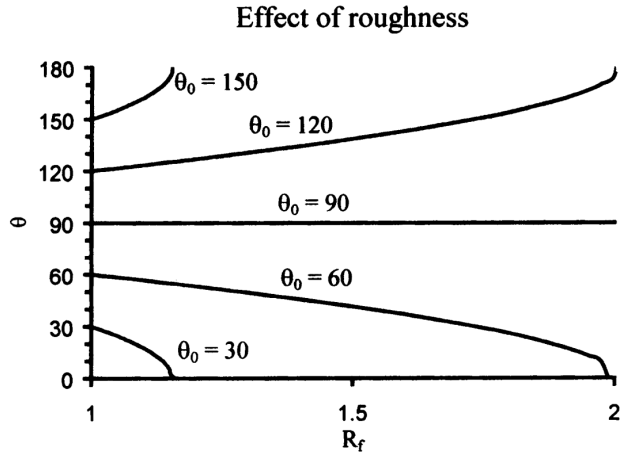


**Figure 2.6:** Contact angle for a rough surface as a function of roughness factor according to Wenzels model<sup>25</sup>



**Figure 2.7:** The Wenzel and Cassie-Baxter models predict that the CA will change as the surface contact area between droplet and substrate, away from the contact line, changes. However, it has been shown that the CA only depends on changes at the contact line.<sup>45</sup>

## 2.2 Water Adhesion

Returning to the topic of biomimetics, the lotus leaf can be characterized as a superhydrophobic surface with a low adhesion to water. Like the lotus leaf, the rose petal shares many of the same surface characteristics, with both surfaces having a micro/nano hierarchical structure giving them contact angles greater than 150°. However, a water droplet on a rose petal will not roll off when tilted. Due to the rose petal having a high adhesion to water a droplet will remain stuck to the surface even when turned upside down. Contact angles alone are therefore not enough to give a detailed picture on superhydrophobicity.

Bhushan and Her sought to explain this mechanism by examining superhydropho-

bic surfaces with differing adhesion values in 2010.<sup>47,48</sup> It was shown that adhesion properties are associated with the wetting state of the droplet. Surfaces with droplets in the Cassie-Baxter state displayed a much lower water adhesion than the droplets in the Wenzel state. As mentioned earlier, the nature of the wetting state is dependent on the total contact area between liquid and solid. Air pockets contribute significantly to a lowering of water adhesion, hence surfaces with deeper microstructures show lower water adhesion than flat surfaces. By varying the surface topography and roughness, surfaces with a high contact angle, but a varying degree of water adhesion have been produced. This was revealed to correlate well with a transition from the Cassie-Baxter to the Wenzel wetting model.<sup>49–51</sup>

To investigate the water adhesion on a surface, several methods have been developed that measure adhesion in different ways. The most common approach is the tilted plate method which examines a droplet on a tilted surface.<sup>52</sup> By increasing the tilting angle, the droplet will eventually slide off when reaching a critical sliding angle. This simple yet effective method has also inspired the development of new similar methods that utilize a centrifugal system or other mechanical ingenuities.<sup>53,54</sup> However, this method only considers adhesion in the lateral direction, parallel to the surface plane. Depending on the direction considered, lateral adhesion force can differ in strength. The most notable example is the directional adhesion of butterfly wings, where a droplet will roll off in one direction, but become pinned in another. This mechanism has allowed the fabrication of ratchet-structured surfaces with anisotropic adhesion behaviour.<sup>55,56</sup>

The normal adhesive force works perpendicular to the surface and can be measured by considering the force required to remove the droplet from the surface. One method involves the use of an atomic force microscope (AFM), by measuring the force between the AFM tip and the substrate surface. However, this method is limited to the submicroscopic level due to the nanoscale size tip, and is insufficient when dealing with microstructured surfaces. Other high-sensitive electromechanical systems exist and have been used with great success for quantitative results on adhesive forces. They usually involve a metal ring with a droplet that is put in contact with a surface. The ring and surface then separate and the adhesive force between them can be measured.<sup>51,57,58</sup>

## 2.3 Superhydrophobic Surfaces

From the principles described in the previous sections an abundant amount of hydrophobic and superhydrophobic surfaces have been fabricated. Aiming to further enhance their water repellent properties, research is focused on the two aspects that govern the Wenzel and the Cassie-Baxter wetting states. Low surface energy coatings reduce the surface energy between the solid and liquid, while the micro/nanostructuring of the surface introduce pockets of air that suspend the droplet.

Several methods have successfully created superhydrophobic surfaces (CAs larger than  $150^\circ$ ), and research is at an all time high with new review articles being published every year, providing an excellent overview of the newest discoveries.<sup>23,24,59-67</sup> The micro/nanostructures and coatings with low surface energy are the two key factors that influence superhydrophobicity. The coatings can be applied by various means, including but not limited to, solution immersion, dip-coating and spin coating.

The method of producing the binary structure, depends entirely on the type of desired structure. With the lotus leaf structure in mind, pillars, rods, spheres and microscale meshes have been fabricated to emulate the micro protrusions of the lotus leaf. For a well-defined pattern which is repeated over a large area, various lithography techniques are preferred.<sup>68,69</sup> Templating or casting processes are similar and involve the copying of a rough surface by use of a soft material that is then hardened. Sun *et al.* used an actual lotus leaf as a template, using it to create a cast out of polydimethylsiloxane (PDMS), which later gave a CA of  $160^\circ$ , in addition to a very low slide off angle.<sup>70</sup> A third method is to use etching, either physical or chemical, and that way create a roughened structure that can be functionalised by for example polytetrafluorethylene (PTFE).<sup>71</sup>

Whether or not superhydrophobic surfaces truly are the best option for icephobic surfaces remains debatable. Various superhydrophobic surfaces have shown to both delay freezing<sup>13,72</sup> and reduce adhesion of ice.<sup>12</sup> However, more recent publications reveal no apparent relation between the two properties, mainly due to the limited durability of the superhydrophobic surfaces.<sup>73-75</sup> Nevertheless, research still continues, perhaps in search of a more thorough understanding of the forces that govern surface interactions.

A common theme of all mentioned fabrication methods in this section is the degrading of an existing flat surface that is made more rough. Another method entirely

concerns the growth of a new material on top of a substrate. A surface of carbon nanotubes can be made this way and these show great promise in superhydrophobicity.

### Superhydrophobic CNT surfaces

CNTs are of immense interest when it comes to superhydrophobic applications. A number of review papers have been written on the topic, but some noticeable results are reviewed below.<sup>76,77</sup> They can easily be grown on both a flat or a textured surface, creating nanostructured features that can replicate the water-repellent properties of the lotus leaf and the self-cleaning properties of the gecko feet.<sup>78,79</sup>

By themselves, CNTs are inherently somewhat hydrophilic,<sup>76</sup> however due to their small cylindrical size they have an exceptionally large length to diameter ratio. Therefore, mixing CNTs with a fluorine terminated hydrophobic coating will greatly increase its water repellent properties, due to the large surface contact area between water droplet and CNT surface.<sup>39,80</sup> In a densely packed porous network of MWCNT, the coating will penetrate and cover the network. However, the surface roughness must still be maintained, too much coating will slowly close the porous network, thus decreasing the water repellency, as observed by Meng and Park.<sup>33</sup> Recently, a superhydrophobic MWCNT structure was grown directly on stainless steel, and even without the use of chemical treatment or functionalisation.<sup>81</sup>

Lau *et. al*<sup>31</sup> prepared vertically aligned carbon nanotubes on silicon, before functionalizing with a nonwetting PTFE coating. This surface showed great superhydrophobic behaviour, with contact angles exceeding 160° in addition to a low water adhesion. Figure 2.8 shows the carbon nanotube forest structure and a water droplet resting on the surface. The excellent water repellent properties are explained by the existence of the Cassie-Baxter state, which trap pockets of air between the CNTs. Therefore, a resting water droplet would be suspended on the surface, while an impacting droplet bounces off.

Zhu *et.al*<sup>82</sup> showed how aligned CNTs with hydrophobic fluorocarbon coating could be grown on microstructured arrays. Even though the CNT nanostructure had a minimal effect on the water contact angle, it did however manage to lower adhesion. On the other hand, superhydrophobic MWCNT surfaces with high water adhesion also been fabricated, evidencing the versatility of these structures.<sup>83</sup>

CNT surfaces hold great promise concerning durability. Luo *et. al*<sup>84</sup> fabricated a flexible CNT-polymer composite film with CAs as high as 165° and sliding angles

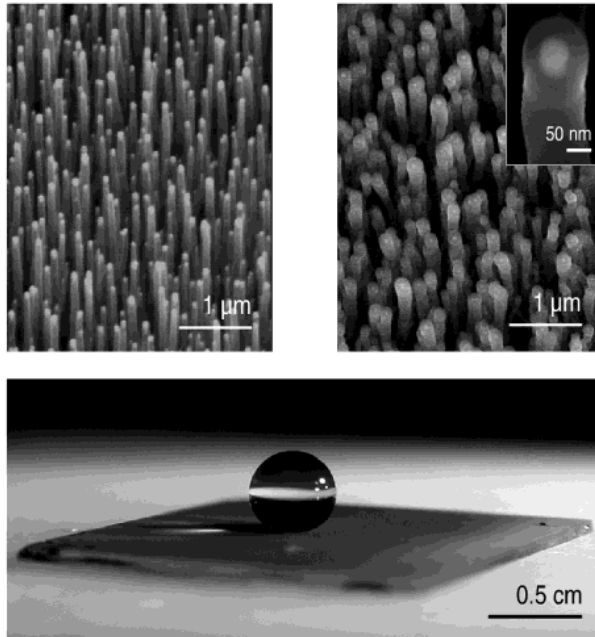


**Figure 2.8:** SEM images of a carbon nanotube forest, with nanotube diameter of 50 nano and height of 2 μm. The surface is able to suspend a droplet on the forest.<sup>31</sup>

less than 4°. These high superhydrophobic properties were retained even after 1000 bending cycles. Similar composites have also been created and deposited on hierarchical, lotus-like structures,<sup>85</sup> with superhydrophobicity compared to structures using lotus wax. The CNT structured showed good mechanical durability, superior to those using lotus wax.

Another issue with previous superhydrophobic surfaces is the effect of condensation on wetting properties. Hierarchical CNT surfaces have shown great promise also in this area by retaining superhydrophobicity after condensation.<sup>86</sup> As seen by figure 2.9, the condensation coalescence occurs on top of the pillars, so that condense can easily be removed and superhydrophobic properties maintained.

An additionally exciting prospect that CNT surfaces offer comes from the intrinsic conductive properties of CNTs. Several researchers have reported the fabrication

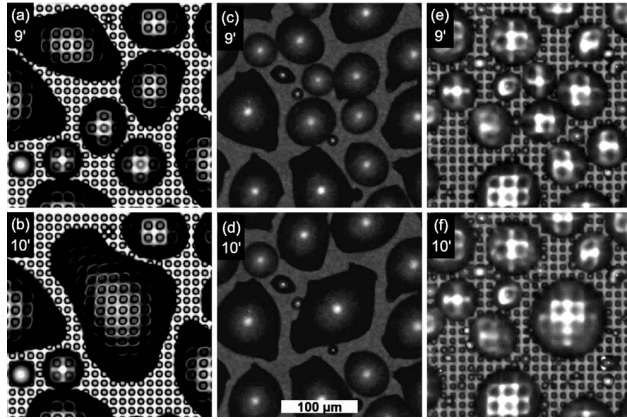


**Figure 2.9:** Coalescence of condensate drops on micro (a)-(b), nano (c)-(d) and hierarchical (e)-(f) structures.<sup>86</sup>

of superhydrophobic, conductive CNTs.<sup>87–89</sup> This property can be utilized by introducing sensors and other electric circuitry on superhydrophobic surfaces for close monitoring and manipulation of the surface. It could also be used for exploring electrically induced reversible transitions between wetting states.<sup>90,91</sup>

Superhydrophobic CNT surfaces have even shown to demonstrate icephobic properties making them a particularly interesting research candidate. One of the few published papers on icephobic CNTs was by Zheng *et. al.*<sup>37</sup> They showed exceptional superhydrophobicity, with CAs in the vicinity of  $170^\circ$ , in addition to icephobic behaviour on cooled, low velocity impacting water droplets. The surface consisted of SWCNTs, functionalized with a low surface energy acetone film.

## Chapter 3

# Carbon Nanotubes

Carbon nanotubes (CNTs) were discovered by chance by Sumio Iijima in 1991 and gained immediate attention because of its unique structure.<sup>92</sup> Not to be confused with the term carbon nanofiber (CNF), which also encompasses filaments of amorphous carbon and stacked graphene layers, a CNT is comprised of tubular graphene walls parallel to the fiber axis<sup>93</sup> (see figure 3.1). Its simplest form is the single wall carbon nanotube (SWCNT), which consists of only one sheet of rolled up graphene, having a diameter usually in the range 1–10 nm, with lengths extending several microns long. Tubes nested inside one another are called multi wall carbon nanotubes (MWCNTs), with diameters that vary greatly. CNTs have gained massive attention in research due to their many unique physical and chemical properties which are of importance in a variety of fields and applications.<sup>94–96</sup>

### 3.1 Fabrication of Carbon Nanotubes

There are several ways of fabricating CNTs, the most common being the arc, laser and chemical vapor deposition techniques. When first discovered by Iijima,<sup>92</sup> the *arc discharge* method was used, a method originally used for the synthesis of the carbon fullerene C<sub>60</sub>. Newer methods have aimed to increase production yield and rate, while at the same time precisely controlling the structure of the tubes. This includes minimising defects, controlling the diameter, length and other features.

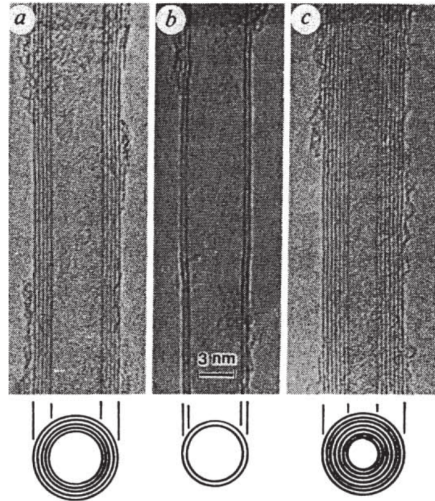


**Figure 3.1:** Transmission Electron Microscope (TEM) images showing how the tubular graphene walls of a carbon nanotube are parallel to the fiber axis.<sup>97</sup>

### Arc Discharge and Laser Ablation

The arc method uses a high electric current through graphitic electrodes in the presence of catalytic particles, producing CNTs and soot. This method can produce large amounts of CNTs and changing the catalyst combination have allowed the production of SWCNTs in addition to the MWCNTs. However, when operating in a highly energetic domain with temperatures often exceeding 3000°C, precise control of the product purity is difficult.<sup>97</sup>

Laser methods involves shooting a laser at a graphite target in the presence of metal catalyst. Carbon will jet out of the target, and will together with the catalyst cool and crystallise into nanoparticles from which SWCNTs grow. Although a reliable method, temperatures are too high to form MWCNTs (~1200°C), and SWCNT are usually formed in tangled structures along with amorphous carbon material.<sup>94,97,98</sup>



## Chemical Vapour Deposition

Chemical Vapour Deposition (CVD) is a more moderate temperature synthesis. It involves the decomposition of a gaseous or volatile carbon bearing gas in chambers heated to between 500°C and 1100°C. These carbon compounds are catalysed by a thin film of metallic nanoparticles which serve as nucleation sites for the initiation of CNT-growth. This synthesis allows for a more precise control of the growth location and is thus the preferred method for high quality tube structures.

One delicate aspect of this method is the size of the catalyst nanoparticles, which need to be of the order of a few nanometers for the synthesis of CNTs. The high temperatures required by thermal CVD (>700°C) also rules out the use of some popular substrate materials, including glass and aluminium. Therefore, plasma enhanced chemical vapour deposition (PECVD) is quickly becoming the favoured method for research purposes.

### Plasma Enhanced Chemical Vapour Deposition (PECVD)

The PECVD process first emerged in microelectronics, as certain circuits could not tolerate the high temperatures of the traditional CVD methods. By using plasma it was possible to bypass this problem completely.

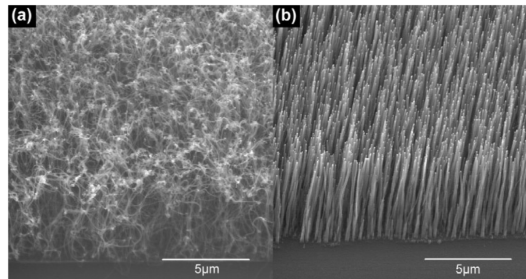


**Figure 3.2:** SEM images showing CNT growth (a) without and (b) with plasma.<sup>99</sup>

Plasma is a highly energised, ionised gas of neutral atoms or molecules, positive ions and free electrons. The energetic plasma is used instead of thermal energy to ionise and excite a source gas during thin film deposition. This is what allows the PECVD to operate between room temperature and 100°C, and why growth can occur

at temperatures as low as (500–700°C), making it the method of choice in IC manufacturing. Growth of CNTs can still not occur below 550°C, but this is still a great reduction compared to the previously mentioned methods. A pair of electrodes maintains an electric field which allows for alignment of the CNTs during growth. This is in contrast to the randomly oriented tubes of thermal CVD (see figure 3.2). With the increased control, there can be deposited free-standing and vertically aligned forests of CNTs. Figure 3.3 shows an example of the precise control of CNT alignment that can be achieved.<sup>100–102</sup>

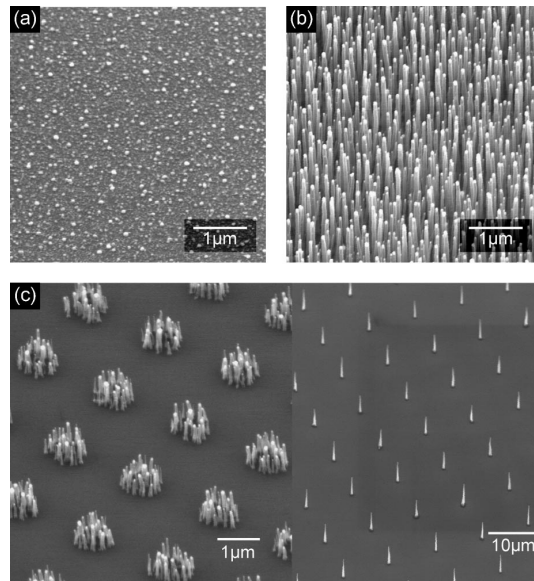


**Figure 3.3:** (a) Nickel catalyst nanoparticles ~50 nm in diameter. (b) Catalysed growth of CNTs, with CNT diameter similar to the nickel particles. (c) Selective growth of areas of CNTs, achieved by patterning the nickel film.<sup>103</sup>

## 3.2 Growth of Carbon Nanotubes

To introduce the necessary catalyst layer for CNT growth, a thin film is usually applied chemically from solution or through thermal evaporation or sputtering. How-

ever, to achieve high yield and uniform growth a diffusion barrier layer is most often applied first, usually an oxide layer. This layer separates the substrate from the active catalyst, thus preserving its activity, avoiding the formation of silicides and other inhibitors of CNT growth.<sup>93, 104–108</sup>

A catalyst thin film is then sputtered or evaporated onto the substrate. The thickness is in the range of a few nanometers, and when heated to the CNT growth temperature, the thin film will break up and coalesce to form nanoclusters. During nucleation, carbon needs to dissolve in the catalyst particle until it reaches saturation and initiates CNT growth. Thus only a limited number of metals are suitable for catalyst use. Fe, Ni or Co are the most reliable ones and are known to be very active in their ability to break and reform carbon-carbon bonds.<sup>94, 106, 109</sup>

The size of the catalyst nanoclusters determine the thickness of the CNTs. For low catalyst layer thicknesses, the tubes are very thin and long and not perfectly aligned. As the thickness increases they become more uniform in diameter, becoming almost perfectly aligned. Too thick layers will result in shorter tubes again, with a large deviation in diameter as can be observed from figure 3.4.

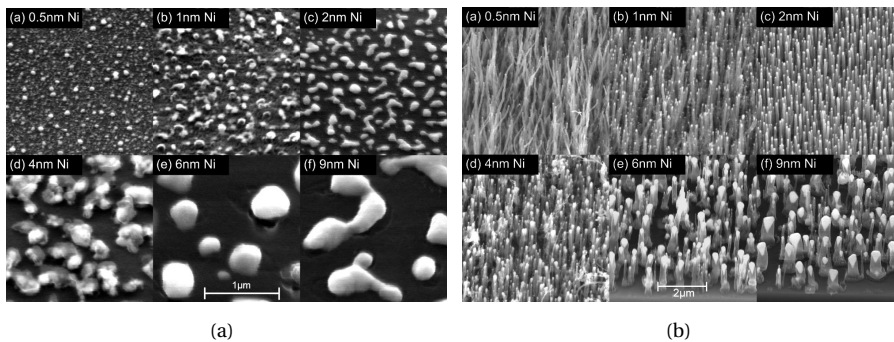


**Figure 3.4:** SEM photographs of (a) sputtered nickel catalyst films with varying thickness after annealing, and (b) CNTs grown on the same nickel layers using the same growth conditions.<sup>104</sup>

The operating conditions of the PECVD will also have a noticeable effect on the finalised CNT surface structure. Apart from the thickness of the initial catalyst film, other parameters that affect the structure include gas flow conditions and temper-

ature in the chamber, as evidenced by figures 3.4-3.6. Regarding gas flow, a large concentration of carbon gas source will result in a large amount of amorphous carbon which overflows the growth of CNTs. Higher temperatures lead to wider tubes or fibers that grow slower.

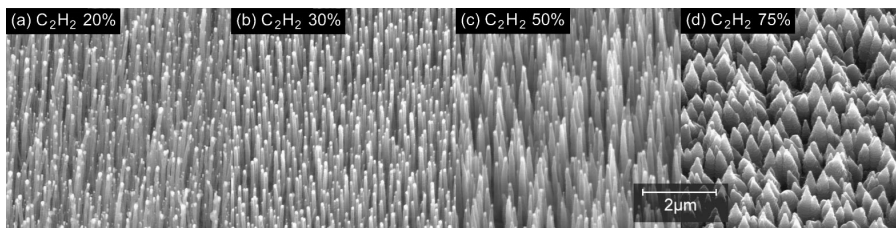


**Figure 3.5:** SEM photographs of CNTs grown at different gas flow concentrations of acetylene.<sup>104</sup>

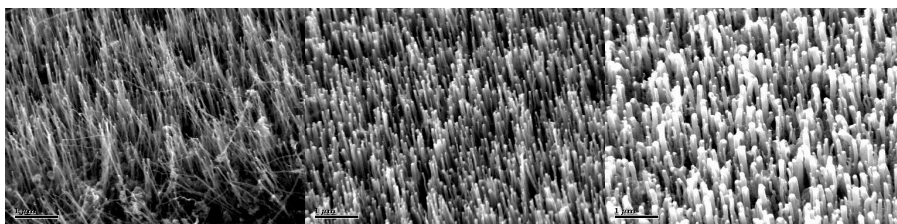


**Figure 3.6:** SEM photographs of CNTs grown at different temperature.<sup>100</sup>

In the PECVD growth chamber, carbon monoxide (CO) or a hydrocarbon such as acetylene ( $C_2H_2$ ), ethylene ( $C_2H_4$ ) or methane ( $CH_4$ ) is usually used as the carbon bearing gas source. Any amorphous carbon is removed by introducing a hydrogen-rich gas such as  $NH_3$  or  $H_2$  during pre-treatment or growth. These react to form volatile C-N and C-H species that remove the excess carbon.<sup>93,99</sup> Sivakumar *et al.* argues that when using  $CH_4$  as the carbon source, a nitrogen-rich atmosphere of either  $N_2$  or  $N_2O$  is preferable, as it maintains the catalytic activity by resisting the reduction of metal oxides due to the resisting nature of  $H_2$ .<sup>110</sup>

The general mechanism of the carbon nanotube growth depends on a number of factors. Nevertheless, the process can be divided into two models, the tip growth

model and the base growth model. For both models, the hydrocarbon gas decomposes on the catalyst particle surface. For the tip growth model, the carbon then either diffuses through or over the surface of the particle, before exiting on the hidden side of the particle. There it forms a nanotube, thus lifting the catalyst particle of the surface as the tube increases in length as can be viewed in figure 3.7. In contrast to this model, where the catalyst particle remain at the top of the tube during growth, we have the base growth model in which the catalyst particle is firmly anchored to the surface of the substrate. The growth of the carbon nanotube occurs on the top, with the nanotube tip free of catalyst particles. With this mechanism, the nanotube will not be able to naturally align vertically by itself as imaged in figure 3.8.<sup>100,104,111</sup>

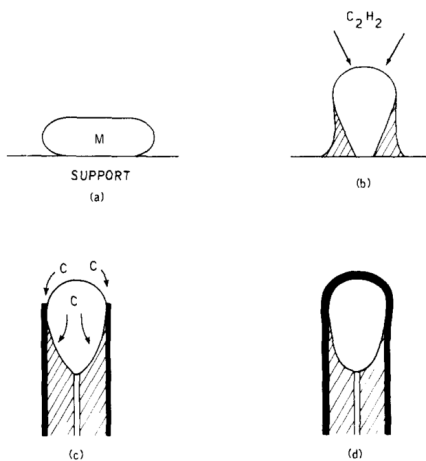


**Figure 3.7:** Mechanism of CNT formation using an acetylene carbon source.<sup>112</sup>

A strong interaction between the support and the catalyst particle favours a base growth model, while a weak adhesion between the two usually results in tip growth. The barrier layer and any treatment to this layer will affect the interaction with the catalyst. In addition to that, for a given barrier layer, research indicates that the growth mode may switch from tip growth for large particles ( $\gg 5$  nm), to base growth for smaller ones ( $< 5$  nm). That might be considered non-intuitive, as a larger, heavier particle would be expected to stick more readily to the substrate, and smaller particles to more readily break off. However, the chemical reactivity of the smaller

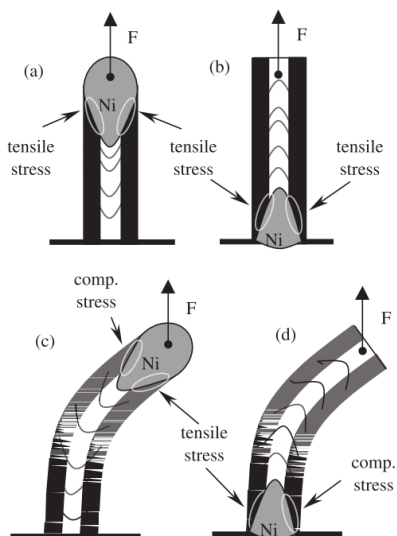


**Figure 3.8:** Influence of the metal-substrate interaction on alignment mechanism.<sup>100</sup>

particles is higher due to the larger surface to volume ratio. That way, carbon growth is initiated sooner (on the surface), in contrast to the larger particles, where carbon first diffuses before growing the nanotube (from below).<sup>113</sup>

# Chapter 4

## Experimental Method

An experimental method was designed and optimised to produce a vertically aligned forest of carbon nanotubes that could be functionalised and tested for water repellent properties. The tubes were grown on a silicon (Si) substrate, using aluminium oxide ( $\text{Al}_2\text{O}_3$ ) as a barrier layer, and iron (Fe) as the catalyst layer. The tubes were functionalised using a solution of perfluorododecyltrichlorosilane (FDTS), and tested for water repellency by measuring contact angles and water adhesive forces.

### 4.1 Fabricating the samples

The method used for fabricating the carbon nanotube surfaces was based on the works by Nordheim and Våland in two earlier master theses from NTNU.<sup>114,115</sup> Nordheims research on the growth and properties of CNTs was performed at NTNU Nanolab, using mostly the same equipment. Altercations to the original recipe have been made based on suggestions and comments from Espen Rogstad of the NTNU Nanolab engineering staff, to accommodate the design needs and requirements of a water repellent surface.

#### Preparing the Samples

The substrate used was a 2 inch, p-type silicon wafer of  $\langle 100 \rangle$  orientation, with a thickness of  $320\mu\text{m}$  to  $350\mu\text{m}$ . Samples of  $1\text{ cm} \times 1\text{ cm}$  were scribed using a Dyna-

tex DX-III scriber unit (Figure 4.1, see figure 4.3 for a scribed sample). To remove any dust or impurity particles that might have accrued, samples were cleaned by immersion in acetone for 1 min, in isopropanol (IPA) for 1 min and then rinsed in deionised (DI) water, before being dried using a nitrogen( $N_2$ )-gun. To remove any residual liquid, the samples were baked at a 180°C hot plate for 90 s. Using a Diener Electronics Femto Plasma Cleaner (Figure 4.1), an  $O_2$ -plasma clean was performed, with a 100 sccm oxygen gas flow at a 50 W power level for 2 min to remove any remaining organic matter.



**Figure 4.1:** The Dynatex DX-III scriber unit (left) was used to scribe samples, while the Diener Electronics Femto Plasma Cleaner (right) performed a plasma clean before metal deposition.<sup>116, 117</sup>

## Deposition of barrier- and catalyst layer

Silicon dioxide is proven to work as a barrier layer for a superhydrophobic CNT surface.<sup>31</sup> However, in this work, aluminium oxide was used, as aluminium is a more industrial applicable material. It also works well with iron based catalysts which are better stabilised compared to silica.<sup>108, 118</sup> In contrast to Nordheims method, where a deposited layer of aluminium was oxidised, the aluminium oxide layer was deposited directly through the use of an AJA Sputter and Evaporator (Figure 4.2). Aluminium was sputtered in an atmosphere of 60 sccm Ar and 6 sccm  $O_2$ , resulting in a 100 nm aluminium oxide barrier layer, with a thickness confirmed through the use of a Filmetrics F20 Reflectometer. The deposition of the aluminium oxide induces a



distinct colour change of the surface, as noticed in figure 4.3. A 3 nm catalyst layer of iron was sputtered using the same machine.

### **Thermal pretreatment and growth of carbon nanotubes**

The thermal pretreatment and the growth of carbon nanotubes was performed in an Oxford Instruments PlasmaLab System 100-PECVD (Figure 4.2). The recipe used had been created by Nordheim and developed further by the NTNU Nanolab engineers.

If the samples were to be characterised by SEM, they would have to be scribed into pieces of about 6 mm×4 mm at this point. By scribing before the CNTs were grown, there was no risk of destroying the vertical aligned tubes at the edges. The samples needed to be this small to fit in the SEM sample holder, and scribing before growth result in more complete images of the cross-section. Scribing is done by using a hand-held scriber pen while the sample is held down using a clean glass slide.

Resting on a 4 inch silicon carrier wafer, the sample was inserted into the PECVD chamber at 650°C. A 2 min purge in 1500 sccm N<sub>2</sub>, followed by a 3 min pump readied the chamber before pumping to a base pressure of  $5 \times 10^{-6}$  mTorr. A 30 min thermal pretreatment period with 50 sccm N<sub>2</sub>O prepared the chamber before introducing the hydrocarbon gas. For 120 min, a gas flow of 50 sccm CH<sub>4</sub> was used to grow the carbon nanotubes, this time is later referred to as the growth time. The 100 W plasma power ensured alignment of the tubes. A new series of N<sub>2</sub>-purging and pumping was then repeated three times while the temperature returned to 300°C, ending with a final pumping to base pressure. The pressure was kept at 1000 mTorr during pretreatment and CNT growth, and at 1500 mTorr during the nitrogen purge. The finalised sample has a recognizable black, soot coloured surface as seen in figure 4.3.

### **Functionalisation**

An oxygen plasma treatment of CNTs was done in the Diener plasma system under 80 W power and with a 25 sccm oxygen gas flow, for 30 s. The amorphous carbon was oxidised and evaporated as CO<sub>2</sub>, while the concentration of C–C and O–C=O bonds on the tubes increased, making them more receptive for further functionalisation.<sup>121–123</sup> The hydrophobic surface functionalisation was done using FDTS,

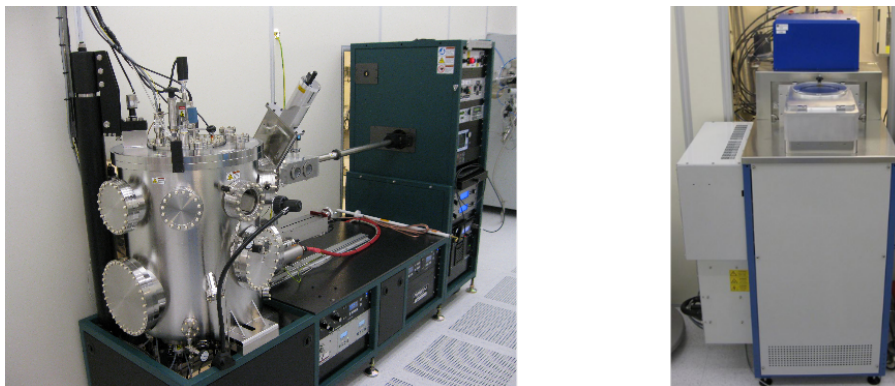


**Figure 4.2:** The AJA Sputter and Evaporator (left) was used for the deposition of a barrier layer and the metal catalyst layer. The Oxford Instruments PECVD (right) used a carbonaceous gas source and plasma to grow the carbon nanotubes.<sup>119, 120</sup>

which has been shown to work very well with carbon-based surfaces before, both graphene<sup>35</sup> and CNTs.<sup>33, 34, 39</sup> The CNT surface was immersed in a 0.5 wt % hexane solution of FDTS at room temperature for 45 min, and then baked in a Termaks TS 8056 Drying Oven at 110°C for 1 h.<sup>124</sup> This ensured a complete distribution and reaction of FDTS at the surface, while the drying allowed for the evaporation of any remaining liquids, thus concluding the sample fabrication.

## 4.2 Characterisation

The nano-/microstructure of the CNT surface was examined by cross-sectional imaging using the scanning electron microscope (SEM) on a Hitachi S-5500 S(T)EM (Figure 4.4). The standard acceleration voltage and beam current used were 10 kV and 10  $\mu$ A respectively. Only very small samples could be characterised, and they would have to be handled with utmost care to avoid damaging the surface structure. The Hitachi S-5500 also has an attached Bruker energy-dispersive X-ray spectroscopy (EDX) system, optimised for the S-5500 which can use x-rays to analyse the elemental composition of a surface.

A JEOL JEM-2100F Transmission Electron Microscope (TEM) with a 200 kV Schot-

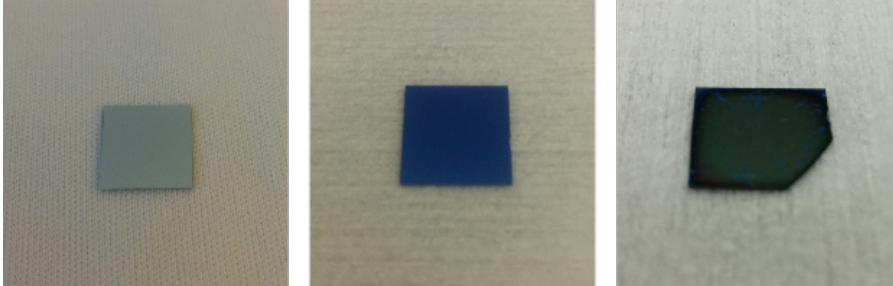


**Figure 4.3:** Scribed silicon sample ready for processing (left). The deposited aluminium oxide barrier layer leaves a noticeable change in colour (middle). After PECVD processing the sample is black because of the CNTs (right).

ky field emission gun was used for a closer investigation of the physical structure of single carbon nanotubes (Figure 4.4). The high resolution images were captured with a Gatan 2k UltraScan CCS camera. To prepare the TEM specimen, CNT samples were soaked in an ultrasonic ethanol bath for 30 min to disperse the nanotubes. A drop of this mixture was then placed on a holey gold grid and allowed to dry before investigation. The specimen preparation, operation of the TEM and image acquiring was performed by a fellow master's student, Aleksander B. Mosberg.

### 4.3 Testing

To examine the water repellent properties of the samples, contact angles and water adhesive forces on the surface was measured.

#### Contact Angle Measurement

Using a microsyringe, a 3–5  $\mu\text{L}$  droplet of deionised water was gently deposited on a fabricated sample. The contact angles were measured using a video-based optical contact angle-measuring device (CAM 200 contact-angle system). Typical contact angle measurement errors were  $\sim 4^\circ$ .



**Figure 4.4:** The Hitachi S-5500 S(T)EM (left) was the primary characterisation instrument used. A JEOL JEM-2100F TEM (right) similar to the one at NTNU was used for high magnification imaging by TEM.<sup>125, 126</sup>

## Water Adhesion Measurement

The normal adhesive force was measured using a high-sensitivity microelectromechanical balance system (DCAT 11 from DataPhysics Instruments GmbH<sup>127</sup>). A  $2.5\ \mu\text{L}$  droplet of deionised water was deposited on a hydrophilic metal ring, fixed to a cantilever. The force of this balance system was initialised to zero while the stage and sample surface was raised towards the droplet at a speed of  $0.05\ \text{mm s}^{-1}$ . Upon contact between droplet and sample surface the stage would stop, and start to move downwards at a speed of  $0.01\ \text{mm s}^{-1}$ . The force exerted on the cantilever was measured until the droplet broke off and was no longer in contact with the surface. Figure 4.5 illustrates the experimental set-up and operation.

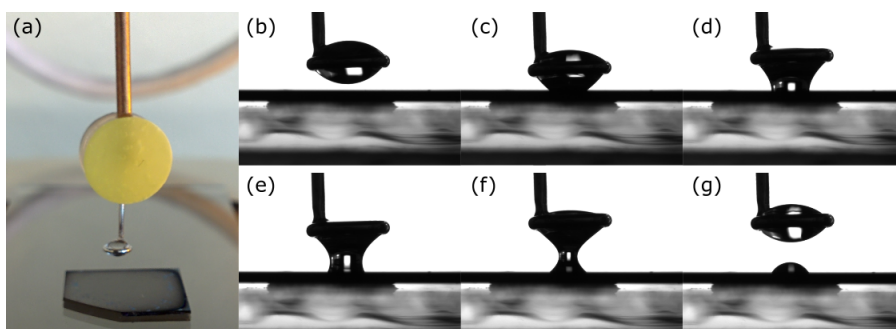


**Figure 4.5:** (a) Image of the experimental set-up with metal ring, droplet and CNT surface. Figures (b)–(g) show six snapshots taken during operation of the instrument.



# Chapter 5

## Results and Discussion

Achieving consistent results using the experimental method detailed in chapter 4 proved to be a challenge. On several occasions, the PECVD process would not give growth of carbon nanotubes. On the rare chance that CNT growth was managed, tube characteristics were distinctly different from those on other processed samples. Tube height would vary from 500 nm to 5  $\mu\text{m}$  even though the process parameters remained the same. This severely limited the ability to optimize the experimental procedure and to increase the output volume of treated samples.

As a result, only a minimal number of samples could be tested for water repellent properties. These samples were mostly the very small specimen used for SEM characterisation, thus restricting the type of measurements that could in fact be performed on the samples. Nevertheless, the samples that were tested showed an excellent surface structure, and were sufficient to develop an informed opinion on the wetting qualities of functionalised CNTs.

### 5.1 Characterisation

#### Structure analysis of carbon nanotubes by SEM and TEM

The scanning electron microscope was the primary tool for characterisation and offered a reliable inspection of the processed samples. Cross-sectional SEM images were taken after each PECVD trial to confirm that the experimental procedure con-

tributed to the desired result. These images formed the basis for any changes that were made to the operating conditions, and ensured a continuous improvement on the structural stability of the CNT surface. Early experiments used PECVD growth times of both 1 h and 1.5 h, but these times proved insufficient as they did not provide the required amount of gas to initiate growth. Hence, a 2 h growth time was primarily used. The SEM was also used to analyse the effect of changing the thickness of the iron catalyst layer. However, due to the aforementioned irregularities with the PECVD, it was not possible to pinpoint the direct effect of a changing catalyst layer thickness, as the variation in the results were too large. The few successfully grown samples had a catalyst layer of about 3 nm. The cross-sectional SEM images of an assortment of samples can be viewed in figure 5.1.

From the 15° tilted view in figures 5.1(a)–(b) the surface topography is clearly visible. The surface is uniform, with only the nano asperities of the CNTs contributing to the roughness. The cross-sectional images in figures 5.1(c)–(d) show a structure height of 5  $\mu\text{m}$ . The catalyst layer thickness and PECVD growth time was predicted to control this. Unfortunately, no such relation was observed, with tube heights varying even when keeping other process parameters constant. The vertical alignment of the tubes is unmistakable and assumed to permeate the bulk of the CNT surface. Due to edge effects, some of the outer tubes are curled up, and these have been more closely examined in figures 5.1(e)–(f). The tube diameter appear to range from about 8 nm to 50 nm, and they are nearly transparent, as tubes can be noticed underneath one another. This suggests that the tubes are nanotubes and not nanofibers, a feature which was later confirmed by TEM images.

Transmission Electron Microscopy made possible the examination of single carbon nanotubes at the atomic level. From figure 5.2 the tube walls can be observed as lines parallel to direction of growth, evidencing their nanotube nature. The existence of more than one tube wall confirm that the tubes are multi-walled (MWCNTs) rather than single-walled (SWCNTs). A intensity spectrum was performed perpendicular to the tube axis to analyse the number of walls in a single tube. The tube composition of 5.2(a) and (b) can be more closely investigated in figure A.1 in appendix A. The tubes have about 15 and 19 walls, with an interatomic distance between walls of about 3.5  $\text{\AA}$  to 4  $\text{\AA}$ . The tubes appear hollow, with no wall structures noticeable in the middle. The TEM images also provide insight to the growth mechanism of the tubes. Catalyst particles (dark spots) were observed at some tips (5.2(e)),



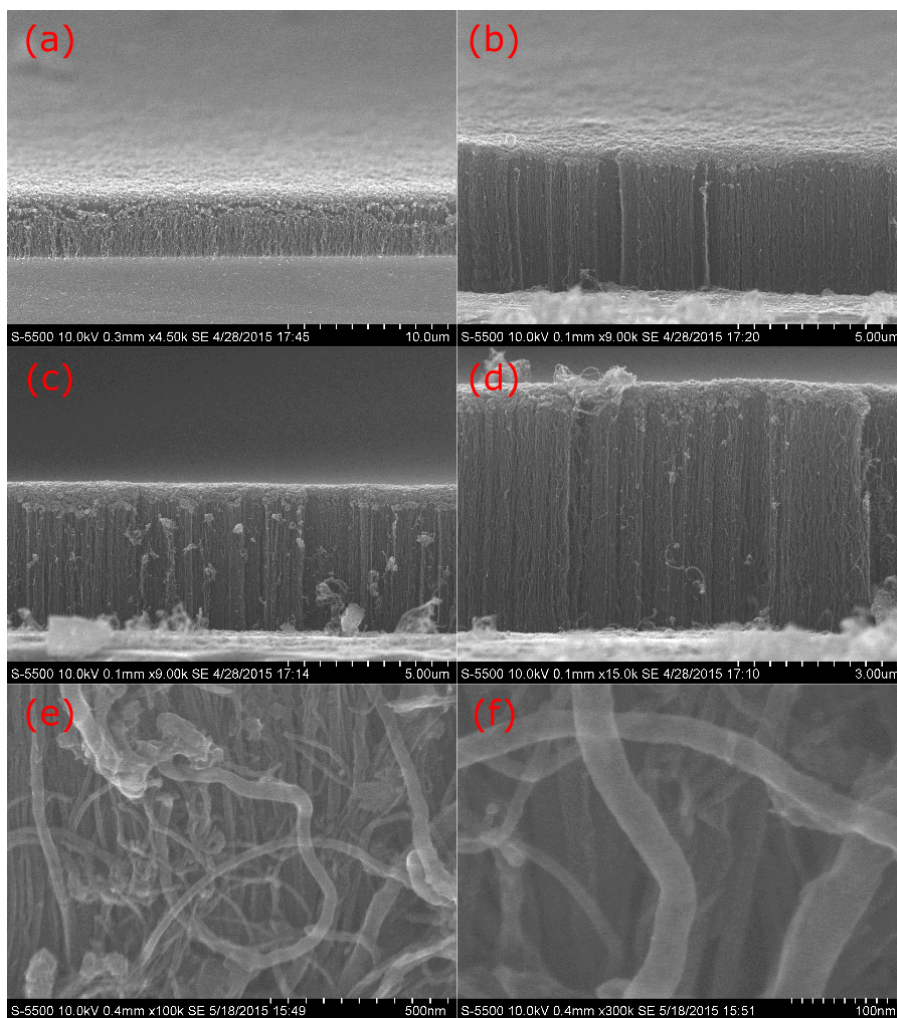


**Figure 5.1:** SEM micrographs of grown carbon nanotube structures. (a)–(b) A 15° tilted view of the CNT surface cross-section with respective magnifications of x4.5k and x9.0k, and scale bars of 10 μm and 5 μm. (c)–(d) Cross-sectional images with respective magnifications of x9.0k and x15.0k, and scale bars of 5 μm and 3 μm. (e)–(f) High-magnification SEM images of carbon nanotubes with respective magnifications of x100k and x300k, and scale bars of 500 nm and 100 nm.

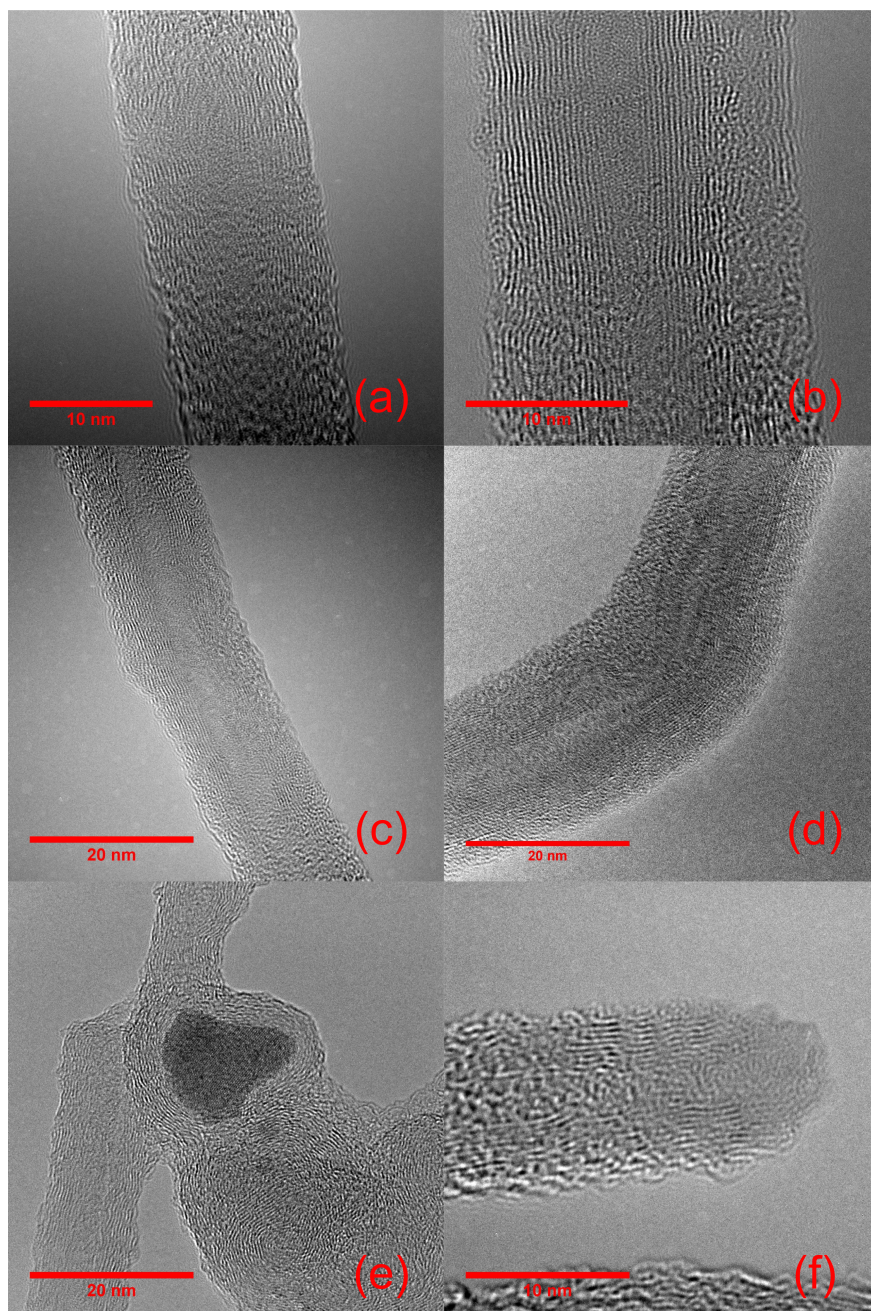


**Figure 5.2:** TEM micrographs of a selection of carbon nanotubes. The tubular walls are clearly visible in (a)–(d). A catalyst particle and a catalyst-free tip can be examined in (e)–(f) respectively. Magnification and scale bars are (a) x500k/10 nm, (b) x800k/10 nm, (c)–(e) x400k/20 nm, (f) x800k/10 nm.

suggesting a tip-growth mechanism. However, many tube ends were also missing catalyst particles (5.2(f)). The growth is hence suspected to be a mixture of both types of growth mechanisms.

### **Structural effect of O<sub>2</sub> plasma treatment and FDTS functionalisation**

The SEM was also used to inspect the effect O<sub>2</sub> plasma treatment and FDTS functionalisation would have on the structure of the grown CNTs. The images in figure 5.3 provided one of the earliest lessons on the effect of O<sub>2</sub> plasma treatment on CNTs. These images show a surface exposed to a 5 min treatment, which is much longer than the 30 s treatment that was used for later samples. Figures 5.3(b)–(c) are from the same area as figures 5.1(c)–(d), and thus offers a unique comparison. The treated structure show a significant change on the tube structure, which appear to be damaged by the O<sub>2</sub> plasma. Following this observation, the treatment time was reduced to 4 min, and then in the end to as little as 30 s, to avoid this damaging effect of the tubes.

It was important to get a clear idea of how the FDTS affects the surface structure of the CNTs. Figure 5.4 show the effect of FDTS functionalisation on four surfaces with the FDTS immersion-time varied from 10 min to 45 min. The FDTS is observed to gather as flakes on the CNT surfaces, but have no apparent effect on the surface structure, which remains intact. There is a variation in the volume of flakes on each surface, with an abundant amount in 5.4(c), but barely any on 5.4(b). The results do not suggest that a longer immersion time give a larger accumulation of flakes, although that might be the intuitive thinking. Since the FDTS did not corrupt the structure, the decision to use a 45 min immersion time for the final samples was based on the measurement of wetting properties.

### **Elemental mapping by EDX**

A cross-section of a CNT-surface was analysed by Energy Dispersive X-ray Spectroscopy (EDX) to examine the elemental composition of the surface. Figure 5.5 shows a SEM image of the analysed cross-section, along with a selection of the most common elements identified by the EDX. As expected, a distinct map of silicon forms around the substrate area, and a thin line of aluminium is observed where

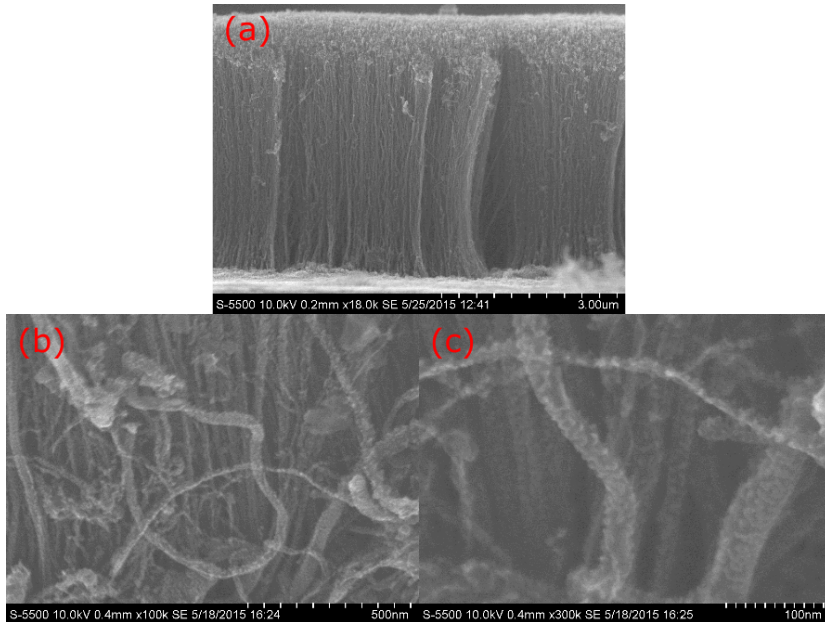


**Figure 5.3:** SEM micrographs of the CNT surface after being treated with  $O_2$  plasma. (a) The surface show little change at a x18.0k magnification, however in (b)–(c), the area from figure 5.1(e)–(f) is inspected, showing surface damage on the exact same nanotubes imaged earlier.

the barrier layer has been grown. Iron and carbon are evident throughout the structure. The concentration of iron is recognized to be higher at the top and bottom of the CNT structure. This further backs the theory that the growth mechanism is a mixture of the two growth models explained earlier.

For the base growth model, iron will remain on the substrate, while for the tip growth model, iron is lifted by the carbon nanotube. Upon closer inspection, one could argue that the concentration of iron is higher at the bottom. In contrast, the concentration of carbon is highest at the top. For the base growth model, growth will halt once carbon can no longer reach the catalyst particle. Carbon might then accumulate on top of the structure, explaining why such a layer is observed on this sample. For base growth to dominate, the iron catalyst would have had to interact

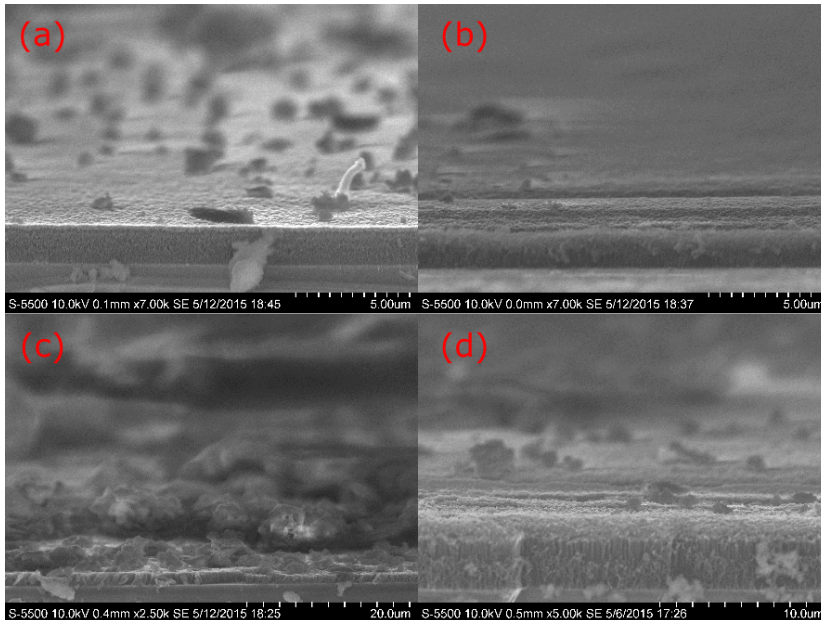


**Figure 5.4:** SEM micrographs of four samples, showing how FDTs accumulates on the surface. Magnification and scale bars are (a)–(b)  $\times 7.0\text{k}/5\ \mu\text{m}$ , (c)  $\times 2.5\text{k}/20\ \mu\text{m}$  and (d)  $\times 5.0\text{k}/10\ \mu\text{m}$ .

more strongly with the aluminium oxide barrier layer. Hence it is more difficult for the catalyst particle to let go of the substrate, and instead it stays and grows the nanotube from the base.

The interaction with the barrier layer might be stronger than expected if the barrier layer is not in fact pure  $\text{Al}_2\text{O}_3$ . The gas flow of  $\text{O}_2$  during deposition in the AJA sputter was set by the NTNU Nanolab engineers, but if it is indeed too low, the true stoichiometry of the barrier layer is not known. It might have a larger concentration of pure aluminium, which would explain the stronger interaction with the iron catalyst layer. To test this hypothesis, some samples with a sputtered barrier layer were oxidised in a Thermcraft Calcination Furnace. However, due to unforeseen events, an exhaust tube on the furnace melted, and this topic was not explored further.

Even though there seems to be an overweight of tubes grown by base-growth (as

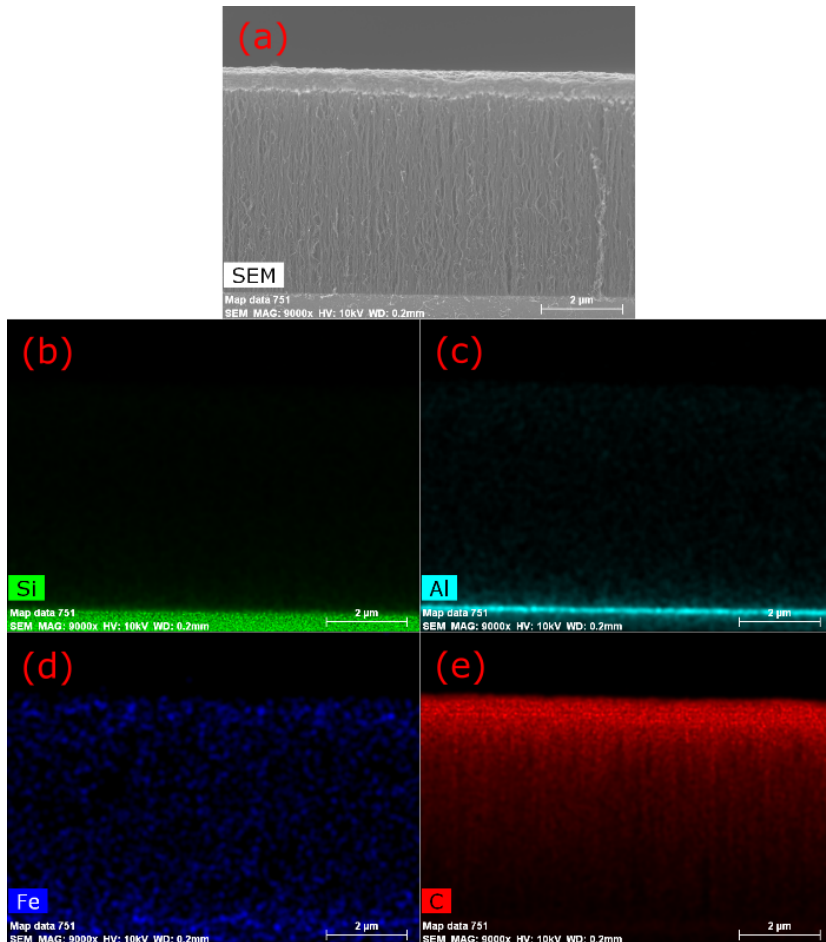


**Figure 5.5:** (a) SEM image of a structure cross-section that has been analysed by EDX. EDX shows the elemental concentration of (b) silicon, (c) aluminium, (d) iron, and (e) carbon.

evidenced by TEM-images and EDX-measurements) the nanotubes are still vertically aligned. The plasma of the PECVD is the greatest contributor to this observed effect, but a portion is most likely kept aligned by the crowding effect of neighbouring tubes alone. Patterning the metal catalyst could potentially provide some interesting insight to the true nature of the CNT alignment.

## 5.2 Water Repellency

The results for the contact angle and water adhesion measurements can be seen in table 5.1. Different surfaces where tested, including an aluminium surface without any carbon nanotubes. The remaining samples all had a grown structure of CNTs on them, but by investigating surfaces with various treatment times of O<sub>2</sub> plasma and FDTS, the wetting properties could be optimised. The contact angle measurements are also summarised in figure 5.6 which show the photographs of a droplet resting on each surface. The adhesive forces are extracted from the force curve of each surface. The force curve of surface 2 can be examined in figure 5.7, while the remaining curves can be viewed in figure B.1 in appendix B.

**Table 5.1:** The water repellent properties of the tested surfaces are summarised in this table.

No.	Surface Composition	Contact Angle [°]	Maximum Force [μN]	Snap-In Force [μN]
1	Al <sub>2</sub> O <sub>3</sub>	68.8	474.6	339.9
2	CNTs	42.8	831.6	670.6
3	CNTs and FDTS, 10 min	75.9	498.5	177.1
4	CNTs and FDTS, 20 min	77.0	467.7	319.3
5	CNTs and FDTS, 30 min	90.4	421.3	352.5
6	CNTs and FDTS, 45 min	90.9	418.5	350.6
7	CNTs, O <sub>2</sub> , 5 min	0.0	580.0	537.1
8	CNTs, O <sub>2</sub> , 4 min and FDTS, 45 min	69.6	422.2	346.9
9	CNTs, O <sub>2</sub> , 30 s and FDTS, 45 min	130.0	279.3	157.5

### Contact Angles

Surface 1 is the silicon substrate with only a 100 nm Al<sub>2</sub>O<sub>3</sub> deposited. A CA of only 68.8° indicate a slightly hydrophilic tendency, likely due to it being a smooth, flat

surface without any other treatment to it. CNTs are inherently hydrophilic, and the CNT surface (2), without any other processing to it, had a CA even lower than 1. Surfaces 3–6 are the CNT surfaces treated with four different FDTS immersion times. The 45 min immersion time gave a slightly larger CA than the others and this time was therefore also used for the remaining samples. The CNT surface that was only treated with O<sub>2</sub> plasma (7) showed superhydrophilic properties, and it was not possible to perform a proper CA measurement, as the water covered the whole surface area. This surface is therefore also the only one not included in figure 5.6.

Surfaces 8 and 9 represent two surfaces that finished the complete process. As described in the previous section, a 5 min plasma treatment executed too much damage to the CNT structure. As a response, the treatment time was reduced to 4 min for surface 8. However, the CA of 8 was about the same as 1, thus no improvement had been made on the original surface. The hydrophilic nature of the O<sub>2</sub> plasma treatment still dominated, and even with the FDTS immersion, the surface remained hydrophilic. For 9, the O<sub>2</sub> plasma treatment time was reduced to 30 s, thus avoiding damage to the tubes, but still maintaining a surface receptive to FDTS functionalisation. This surface was nearly superhydrophobic, achieving a CA of 130°. This compares to the hydrophobicity of some other CNT surfaces,<sup>34</sup> but it is still not high enough to be classified as a superhydrophobic CNT surface.<sup>31,81</sup>

## Water Adhesion

The adhesive forces summarised in table 5.1 are derived from the graphs on water adhesion. The graph of surface 9 can be seen in figure 5.7, while the remaining graphs are summarised in figure B.1. Samuel *et al.*<sup>58</sup> suggest that the snap-in force and pull-off force are the most relevant to water adhesion. The snap-in force is believed to measure the attractive wetting force when the water droplet first interacts with the surface and has been included in table 5.1. The pull-off force is not included in this thesis as that was not always recorded properly for all measurements. The maximum force is included. Figure 5.7 indicates where on the curve the forces are recorded (snap-in force at point 1, and maximum force at point 2).

The adhesive force is believed to correlate well with the wetting state of the droplet. For a high adhesive force the Wenzel state dominates, while the Cassie-Baxter model is more common for low adhesion surfaces. However, all the surface exhibit relatively high water adhesion, suggesting that they are all wetted in the Wenzel state, or



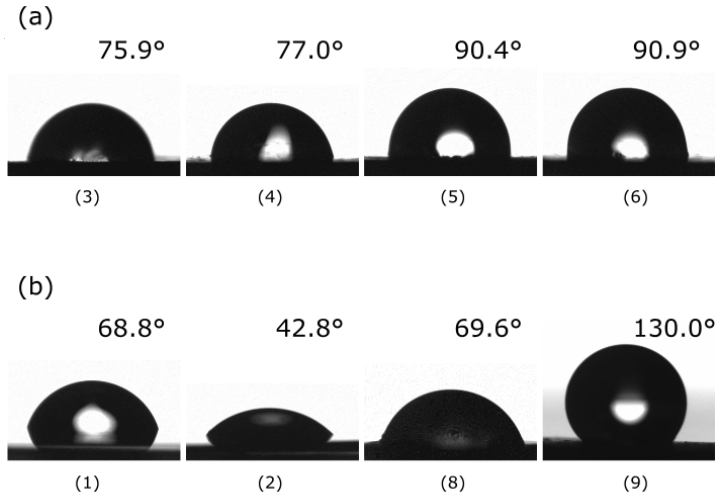


**Figure 5.6:** The contact angles of the tested surfaces are shown in this figure. Consult table 5.1 for a detailed description of each surface composition. The effect of a longer FDTS immersion time is illustrated in (a), with a longer immersion time leading to a higher CA. The remaining samples (except 7, which could not be measured) can be viewed in (b).

at best a mixed state. They all leave a residual droplet on the surface after testing, an indication of a high adhesion to water.

Surfaces **2** and **7** have the lowest CAs and also the highest water adhesion values. This is as expected since carbon and oxidised carbon is hydrophilic. On these surfaces, water is allowed to penetrate the asperities of the CNTs. The surfaces that are covered in FDTS show distinctly lower adhesive force values, primarily because of the hydrophobic nature of FDTS. It is observed that **3** has a very low snap-in force, however, the adhesive force reaches a much higher maximum value. From figure 5.8 the linear relation between the maximum force and the snap-in force can be investigated. Surface **3** deviates from this relation, a possible explanation is that the droplet transitions from a low adhesion Cassie-Baxter state to the Wenzel state during the experiment.

The high CA surface **9** shows the lowest adhesion value, but still a residual droplet

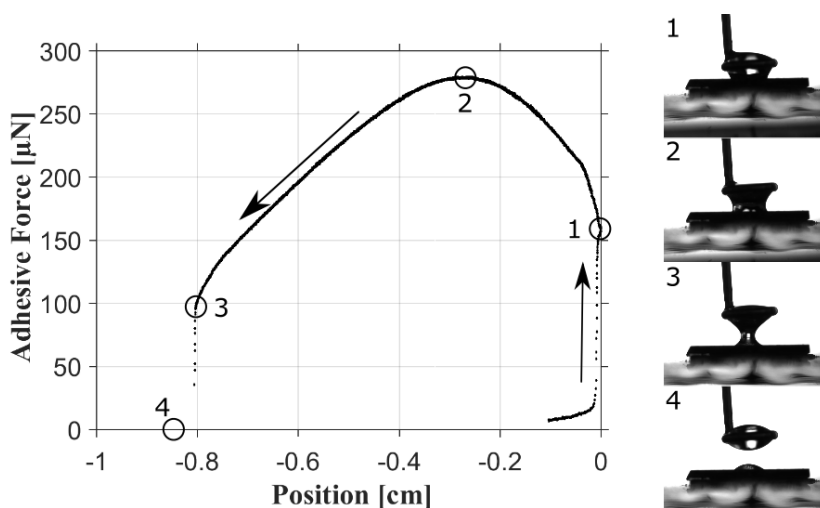


**Figure 5.7:** The adhesive force curve of surface **9** is shown in this figure. It represents the movement of the sample stage towards the ring with the droplet and the subsequent withdrawal of the stage upon contact (direction of the arrows). The snap-in force is recorded at point 1, which is where the stage first contacts the droplet. When withdrawing, the adhesive force reaches a maximum at point 2, before withdrawing further until it pulls off at point 3. At point 4, a small droplet still remains on the surface.

remains after testing. Although the surface has a high CA, its wetting behaviour seem to resemble more that of a rose petal than that of a lotus leaf. Although the adhesion force is high, it has still seen a decrease compared to the original aluminium covered surface. Compared to the untreated CNT surface, the decrease is even greater. There has been no change in the structure between surface **2** and **9**, suggesting that the primary reason for an increased CA and a decreased adhesive force, is the functionalisation of  $O_2$  plasma and FDTS. When comparing surfaces **6** and **9** the importance of the role of  $O_2$  plasma is evident as the adhesion is reduced just with the addition of the oxygen treatment.

Had **9** been compared with a *tenth* surface consisting of flat amorphous carbon treated with  $O_2$  plasma and FDTS, it would have been possible to more accurately determine the true effect of the CNT structure on wetting. Nevertheless, as flat sur-

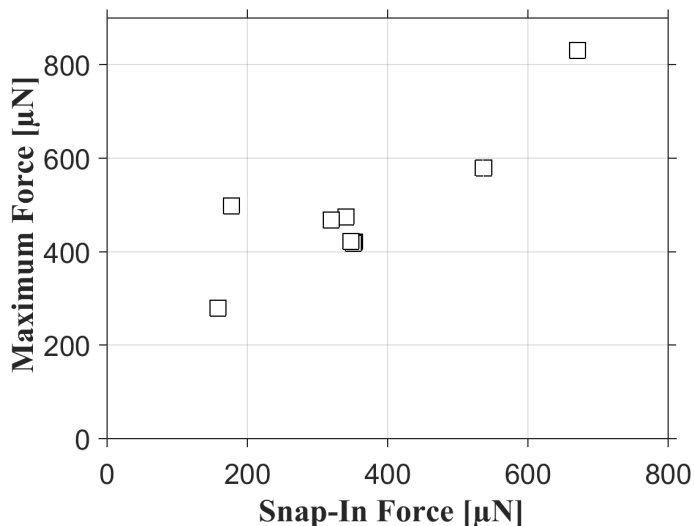


**Figure 5.8:** The adhesive force from table 5.1 are plotted against each other in this figure. The relationship shows a good linear correlation between the two forces, indicating that there is no reason for considering both forces separately.

faces seldom reach CAs as high as  $130^\circ$  it can be safely assumed that the roughness of the CNT structure plays some part in the water repellent properties of **9**. Water is presumed to penetrate the asperities of the nanotube surface, leading to a high water adhesion, but due to the hydrophobic treatment of the surface area a high contact angle is still observed. A higher contact angle could be obtained by a further optimisation of the plasma treatment time and of the FDTS immersion time. Whether or not this would also have an effect on the adhesive forces is not known.

These initial observations suggest that there might be a correlation between the CA and the adhesive force. The two adhesive forces are plotted against contact angles in figure 5.9. An obvious trend can be noticed from this figure, with CA values increasing as adhesive forces decrease. However, due to the limited number of surfaces that have been examined, it is hard to draw a clear connection between the two results.

Considering that a Cassie-Baxter wetting state is not observed, it seems the CNT

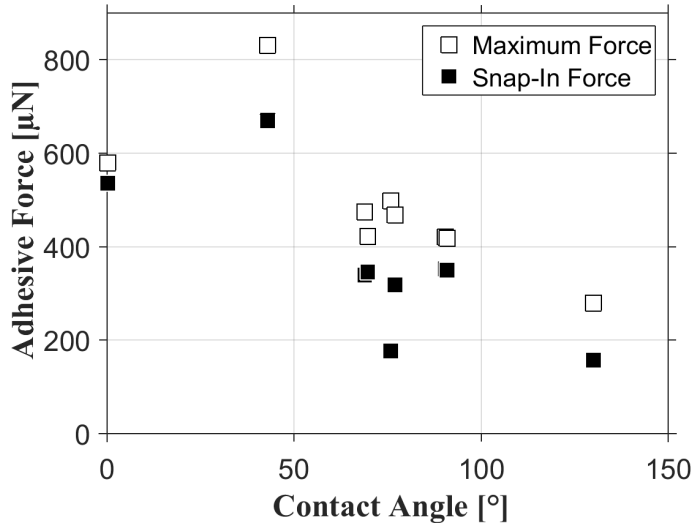


**Figure 5.9:** The two adhesive forces are plotted against the contact angles (values are from table 5.1). A linear trend can be noticed, with the adhesive force decreasing for an increasing contact angle value.

structure has not been able to trap air as it was intended to do. From the surface images in figure 5.1 one could assume that it is only the roughness of the top layer that has an effect, and that the CNT structure in the bulk of the surface is not activated. The structure could be too crowded, such that no air pockets are created in the surface. Judging by the SEM and EDX images in figures 5.1 and 5.5, another reason could be that the observed accumulation of carbon on top of the surface covers the CNTs. This issue is a result of a suboptimal method design, most likely related to the PECVD recipe. Had it not been for the unreliable growth results, more time could have been dedicated to optimising this growth procedure. The recipe uses a gas mixture of  $\text{CH}_4$  and  $\text{N}_2\text{O}$ , but no hydrogen rich molecules such as  $\text{NH}_3$  or  $\text{H}_2$ . This is uncommon, but earlier in the text it was argued that the rich nitrogen atmosphere better maintains the catalytic activity of the iron. What should have been examined is the effect of introducing  $\text{NH}_3$  or  $\text{H}_2$  at a later stage of the recipe. A gas mixture of  $\text{CH}_4$  and  $\text{NH}_3$  would possibly result in a more disperse distribution of CNTs and a

smaller amount of amorphous carbon, more similar to such a structure observed in figure 2.8.

By the results of the water adhesion tests performed by others on the same instrument the water repellent properties can be better assessed. On a superhydrophobic polystyrene layer, water force adhesion measurements gave a snap-in force of  $0\ \mu\text{N}$ , with the pull-off point coinciding with the maximum point at  $60\ \mu\text{N}$ .<sup>57</sup> The same behaviour is observed by Long *et al.*, reporting maximum force adhesion values ranging from  $10\ \mu\text{N}$  to  $110\ \mu\text{N}$ . A more comprehensive study by Samuel *et al.*, compared surfaces of varying degrees of wetting, spanning from hydrophilic to superhydrophobic surfaces (CAs of  $71^\circ$  to  $150^\circ$ ). Recorded snap-in forces were as high as  $470\ \mu\text{N}$ , but still  $0\ \mu\text{N}$  for the superhydrophobic ones. Those were functionalised textured surfaces of silicon pillars with contact angles higher than  $150^\circ$ . The snap-in force of  $157\ \mu\text{N}$  for surface **9**, categorises it amongst the functionalised, untextured surfaces of Samuel in terms of water adhesion, but still closer to the superhydrophobic surfaces in terms of contact angles. This comparison suggests that a different patterning of the CNT surface, or potentially adding the CNT structure to an existing micro structure could potentially decrease the water adhesion force of the surface.

It should be considered that a high water adhesion force is not necessarily only a negative effect. Hydrophobic, high adhesion surfaces serve many purposes, and is still desirable in some applications, such as adhesive tapes. However, for this thesis, where superhydrophobic, self-cleaning properties are desired, water adhesion should be lower. Whether a surface such as this could potentially become icephobic would depend on how much the water adhesion could be improved. With the small water attraction that this surface exerts, it would be very unfavourable in reducing ice adhesion. Wang *et al.* created an ice-phobic surface out of nano-cones that displayed a water adhesion force below  $100\ \mu\text{N}$ . The CNT surface should reach an adhesion force close to this limit if it would be considered for icephobic purposes. The durability of the structure should also be improved, as the carbon was easily removed by simple scratching of the surface. One sample even experienced a swelling effect following the wetting tests as seen in figure 5.10. The effect was visible throughout the surface, but no such thing was observed on other samples.

All these results identify the limits of fabricating a nano-structure alone, without the addition of a micro-structure as well. The lotus-like hierarchical structures consistently achieve better water repellent properties than one simple structure by

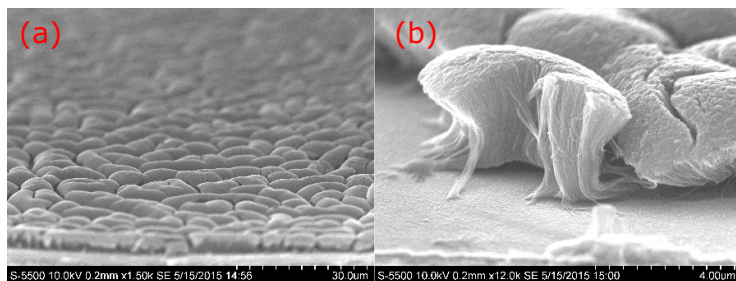


**Figure 5.10:** SEM micrographs of one sample that experienced a swelling effect of the CNT structure following the measurements on wetting. Magnification and scale bar of (a) x1.5k/30 μm and (b) x12.0k/4 μm.

itself. Finishing on a positive note, a CA of 130° is very good, and combining this CNT structure with a micro-structured surface would give a very water repellent surface. Furthermore if the CNT structure was optimised, a hierarchical nano/micro-structure with CNTs would most definitely achieve superhydrophobicity.

## Chapter 6

# Conclusion and Outlook

### 6.1 Conclusion

In this thesis, a surface of vertically aligned carbon nanotubes (CNTs) have been grown by the use of plasma enhanced chemical vapour deposition (PECVD). A 100 nm aluminium oxide layer functions as the barrier layer, while a 3 nm iron layer form the catalyst layer. A 2 h growth in  $\text{CH}_4$  resulted in a uniform structure of multi-walled carbon nanotubes (MWCNTs).

The CNT structure was characterised by the use of a scanning electron microscope (SEM), while single tubes were examined using transmission electron microscope (TEM). The tube structure showed a great vertical alignment, reaching a height of  $5\ \mu\text{m}$ , with tube thickness of 8 nm to 50 nm. The TEM images confirm the nanotube structure, as the tubular walls can be seen parallel to the fiber axis. These images, along with elemental EDX mapping of the surface, indicate that a mixture of the tip-growth- and the base-growth-mechanism has occurred during the CNT growth.

Through a 30 s treatment in  $\text{O}_2$  plasma, followed by a functionalisation with perfluorododecyltrichlorosilane (FDTS), the surface was made hydrophobic. Wetting and adhesion forces between water and the surface were measured, giving a contact angle of  $130^\circ$  and a maximum adhesion force of  $279.3\ \mu\text{N}$ .

These results show a great improvement compared to the initial aluminium sur-

face, in particular with regards to the contact angle. A decrease in the adhesive force is recorded, but the surface still demonstrates an attraction to water. It is argued that this attraction causes water to wet the surface in a Wenzel state, in contrast to the more desired Cassie-Baxter state. Due to the very effective surface treatment by  $O_2$  plasma and FDTS, the contact angle is high, but the CNT protrusions are not able to trap air in the structure for an optimal suspension of the water droplet. Patterning the catalyst layer could provide this property. The nano structure could also be grown on an existing micro structure to get a hierarchical structure, which usually performs better than the two separate surface structures.

## 6.2 Outlook and Further Work

The fabricated functionalised CNT surface shows great promise because of its hydrophobic properties. The functionalisation in particular could potentially be improved even more. A limited number of parameters were tested, and with only three  $O_2$  plasma treatment times, and four FDTS immersion time, there are still potential times that could provide even higher contact angles.

The largest issue is however with the PECVD. On a rare occasion, it did produce some excellent CNT surfaces, but most samples returned from the PECVD chamber without carbon nanotubes. This was unfortunate, because here is where the greatest potential for improvement lies. Once consistent results are acquired, the thickness of the barrier layer and catalyst layer can be varied so that the effect of these changes can be properly measured and understood. The parameters of the PECVD should be looked on as well. The fabricated CNT structure is not able to utilise the true potential of the tubes themselves, as the structure appears to be closed off at the top. A shorter growth time, or a more nitrogen rich growth atmosphere could potentially sort this issue out.

Even with the proposed changes, it remains to be seen if and when such a surface could become industrially applicable. The original purpose of this thesis was to examine the icephobic properties of a CNT surface. However, no large enough samples were fabricated, and this property was never tested. The surface has already demonstrated hydrophobicity, although the water adhesion is considered a bit high. The CNTs are however easily removed by scratching, a poor characteristic for a surface that is required to be long-lasting and durable. With an improved



fabrication design, great potential still awaits such a surface.



# Bibliography

- [1] “Johan Castberg,” <http://www.statoil.com/en/ouoperations/futurevolumes/projectdevelopment/Pages/Skrugard.aspx>, nov 2014, [Online; accessed 02-December-2014].
- [2] “Need more time for Castberg,” [http://www.statoil.com/en/NewsAndMedia/News/2014/Pages/30Jun\\_JCmelding.aspx](http://www.statoil.com/en/NewsAndMedia/News/2014/Pages/30Jun_JCmelding.aspx), may 2014, [Online; accessed 02-December-2014].
- [3] “Gas/oil discovery north of the Snøhvit field in the Barents Sea – 7220/8-1,” <http://www.npd.no/en/news/Exploration-drilling-results/2011/72208-1/>, apr 2011, [Online; accessed 02-December-2014].
- [4] “Oil discovery in the Barents Sea – 7324/8-1,” <http://www.npd.no/en/news/Exploration-drilling-results/2013/73248-1/>, sep 2013, [Online; accessed 02-December-2014].
- [5] “Significant oil and gas discovery northwest of the Snøhvit field in the Barents Sea - 7220/11-1,” <http://www.npd.no/en/news/Exploration-drilling-results/2014/722011-1/>, oct 2014, [Online; accessed 02-December-2014].
- [6] S. H. Eriksen, “Petroleum Resources on the Norwegian Continental Shelf - Exploration,” Norwegian Petroleum Directorate, Tech. Rep., 2013.
- [7] N. E. ASA, “Perspectives for the Barents Sea,” North Energy ASA, Tech. Rep., 2014.
- [8] M. Farzaneh and C. C. Ryerson, “Anti-icing and deicing techniques,” *Cold Reg. Sci. Technol.*, vol. 65, no. 1, pp. 1–4, 2011.

- [9] C. C. Ryerson, "Ice protection of offshore platforms," *Cold Reg. Sci. Technol.*, vol. 65, no. 1, pp. 97–110, 2011.
- [10] S. A. Kulinich and M. Farzaneh, "On ice-releasing properties of rough hydrophobic coatings," *Cold Reg. Sci. Technol.*, vol. 65, no. 1, pp. 60–64, 2011.
- [11] S. A. Kulinich and M. Farzaneh, "How wetting hysteresis influences ice adhesion strength on superhydrophobic surfaces." *Langmuir*, vol. 25, no. 16, pp. 8854–6, 2009.
- [12] S. A. Kulinich and M. Farzaneh, "Ice adhesion on super-hydrophobic surfaces," *Appl. Surf. Sci.*, vol. 255, no. 18, pp. 8153–8157, 2009.
- [13] L. Cao *et al.*, "Anti-icing superhydrophobic coatings." *Langmuir*, vol. 25, no. 21, pp. 12 444–8, Nov. 2009.
- [14] L. Mishchenko, B. Hatton, and V. Bahadur, "Design of ice-free nanostructured surfaces based on repulsion of impacting water droplets," *ACS Nano*, vol. 4, no. 12, pp. 7699–7707, 2010.
- [15] P. Tourkine, M. L. Merrer, and D. Quéré, "Delayed freezing on water repellent materials," *Langmuir*, vol. 25, no. 14, pp. 7214–7216, 2009.
- [16] W. Barthlott and C. Neinhuis, "Purity of the sacred lotus, or escape from contamination in biological surfaces," *Planta*, vol. 202, pp. 1–8, 1997.
- [17] D. L. Hu, B. Chan, and J. W. M. Bush, "The hydrodynamics of water strider locomotion," *Nature*, vol. 424, pp. 663–666, 2003.
- [18] X. Q. Feng *et al.*, "Superior water repellency of water strider legs with hierarchical structures: experiments and analysis," *Langmuir*, vol. 23, pp. 4892–4896, 2007.
- [19] X. Gao *et al.*, "The Dry-Style Antifogging Properties of Mosquito Compound Eyes and Artificial Analogues Prepared by Soft Lithography," *Adv. Mater.*, vol. 19, no. 17, pp. 2213–2217, 2007.
- [20] R. Sandnes, "Wetting Properties of Springtail Cuticles: A Quantitative Analysis," Master's thesis, Norwegian University of Science and Technology, 2012.

- [21] T. Sun *et al.*, "Bioinspired surfaces with special wettability." *Acc. Chem. Res.*, vol. 38, no. 8, pp. 644–52, 2005.
- [22] X. Yao, Y. Song, and L. Jiang, "Applications of bio-inspired special wettable surfaces." *Adv. Mater.*, vol. 23, no. 6, pp. 719–34, 2011.
- [23] X.-M. Li, D. Reinhoudt, and M. Crego-Calama, "What do we need for a superhydrophobic surface? A review on the recent progress in the preparation of superhydrophobic surfaces." *Chem. Soc. Rev.*, vol. 36, no. 8, pp. 1350–68, 2007.
- [24] Y. Zhang *et al.*, "Recent progress of double-structural and functional materials with special wettability," *J. Mater. Chem.*, vol. 22, no. 3, p. 799, 2012.
- [25] B. Bhushan, Y. C. Jung, and K. Koch, "Micro-, nano- and hierarchical structures for superhydrophobicity, self-cleaning and low adhesion." *Philos. Trans. A. Math. Phys. Eng. Sci.*, vol. 367, no. 1894, pp. 1631–72, May 2009.
- [26] E. Bormashenko *et al.*, "Why do pigeon feathers repel water? Hydrophobicity of pennaes, Cassie-Baxter wetting hypothesis and Cassie-Wenzel capillarity-induced wetting transition." *J. Colloid Interface Sci.*, vol. 311, no. 1, pp. 212–6, 2007.
- [27] L. Oberli *et al.*, "Condensation and freezing of droplets on superhydrophobic surfaces," *Adv. Colloid Interface Sci.*, vol. 210, pp. 47–57, 2014.
- [28] S. H. Kim, "Fabrication of Superhydrophobic Surfaces," *J. Adhes. Sci. Technol.*, vol. 22, no. 3-4, pp. 235–250, 2008.
- [29] T. Nishino, M. Meguro, and K. Nakamae, "The lowest surface free energy based on-CF<sub>3</sub> alignment," *Langmuir*, vol. 15, no. 13, pp. 4321–4323, 1999.
- [30] E. Hare, E. Shafrin, and W. Zisman, "Properties of films of adsorbed fluorinated acids," *J. Phys. . . .*, vol. 513, no. 3, pp. 236–239, 1954.
- [31] K. K. S. Lau *et al.*, "Superhydrophobic Carbon Nanotube Forests," *Nano Lett.*, vol. 3, no. 12, pp. 1701–1705, 2003.
- [32] D. Janssen *et al.*, "Static solvent contact angle measurements, surface free energy and wettability determination of various self-assembled monolayers on silicon dioxide," *Thin Solid Films*, vol. 515, no. 4, pp. 1433–1438, 2006.

- [33] L.-Y. Meng and S.-J. Park, "Effect of fluorination of carbon nanotubes on superhydrophobic properties of fluoro-based films." *J. Colloid Interface Sci.*, vol. 342, no. 2, pp. 559–63, 2010.
- [34] I. Y. Y. Bu and S. P. Oei, "Hydrophobic vertically aligned carbon nanotubes on Corning glass for self cleaning applications," *Applied Surface Science*, vol. 256, no. 22, pp. 6699–6704, 2010.
- [35] Y. Lin *et al.*, "Superhydrophobic functionalized graphene aerogels," *ACS Applied Materials and Interfaces*, vol. 3, no. 7, pp. 2200–2203, 2011.
- [36] M. Zhang, T. Zhang, and T. Cui, "Wettability conversion from superoleophobic to superhydrophilic on titania/single-walled carbon nanotube composite coatings." *Langmuir*, vol. 27, no. 15, pp. 9295–301, 2011.
- [37] L. Zheng *et al.*, "Exceptional superhydrophobicity and low velocity impact icephobicity of acetone-functionalized carbon nanotube films." *Langmuir*, vol. 27, no. 16, pp. 9936–43, 2011.
- [38] R. Menini and M. Farzaneh, "Advanced Icephobic Coatings," *J. Adhes. Sci. Technol.*, vol. 25, no. 9, pp. 971–992, 2012.
- [39] L.-Y. Meng and S.-J. Park, "Improvement of Superhydrophobicity of Multi-Walled Carbon Nanotubes Produced by Fluorination," *Carbon Lett.*, vol. 13, no. 3, pp. 178–181, 2012.
- [40] T. Maitra *et al.*, "Hierarchically nanotextured surfaces maintaining superhydrophobicity under severely adverse conditions." *Nanoscale*, 2014.
- [41] R. N. Wenzel, "Resistance of solid surfaces to wetting by water," *Ind. Eng. Chem.*, vol. 28, no. 8, pp. 988–994, 1936.
- [42] A. Cassie and S. Baxter, "Wettability of porous surfaces," *Trans. Faraday Soc.*, vol. 40, pp. 546–551, 1944.
- [43] J. Bico, U. Thiele, and D. Quéré, "Wetting of textured surfaces," *Colloids Surfaces A Physicochem. . . .*, vol. 206, pp. 41–46, 2002.
- [44] C. W. Extrand, "Contact Angles and Hysteresis on Surfaces with Chemically Heterogeneous Islands," *Langmuir*, vol. 19, no. 9, pp. 3793–3796, 2003.

- [45] L. Gao and T. J. McCarthy, "How Wenzel and Cassie were wrong," *Langmuir*, vol. 23, no. 7, pp. 3762–5, 2007.
- [46] L. Gao and T. J. McCarthy, "Wetting 101°," *Langmuir*, vol. 25, no. 24, pp. 14 105–15, 2009.
- [47] B. Bhushan and E. K. Her, "Fabrication of superhydrophobic surfaces with high and low adhesion inspired from rose petal," *Langmuir*, vol. 26, no. 11, pp. 8207–8217, 2010.
- [48] B. Bhushan and M. Nosonovsky, "The rose petal effect and the modes of superhydrophobicity," *Philosophical transactions. Series A, Mathematical, physical, and engineering sciences*, vol. 368, no. 1929, pp. 4713–4728, 2010.
- [49] Y. Lai *et al.*, "Markedly controllable adhesion of superhydrophobic spongelike nanostructure TiO<sub>2</sub> films," *Langmuir*, vol. 24, no. 8, pp. 3867–3873, 2008.
- [50] J. Li *et al.*, "Fabrication of superhydrophobic CuO surfaces with tunable water adhesion," *Journal of Physical Chemistry C*, vol. 115, no. 11, pp. 4726–4729, 2011.
- [51] J. Long *et al.*, "Superhydrophobic Surfaces Fabricated by Femtosecond Laser with Tunable Water Adhesion: From Lotus Leaf to Rose Petal," *ACS Applied Materials & Interfaces*, vol. 7, no. 18, pp. 9858–9865, 2015.
- [52] C. G. L. Furmidge, "Studies at phase interfaces. I. The sliding of liquid drops on solid surfaces and a theory for spray retention," *J. Colloid Sci.*, vol. 17, pp. 309–324, 1962.
- [53] R. Tadmor *et al.*, "Measurement of lateral adhesion forces at the interface between a liquid drop and a substrate," *Physical Review Letters*, vol. 103, no. 26, pp. 1–4, 2009.
- [54] J. M. Lee, S.-h. Lee, and J. S. Ko, "Dynamic lateral adhesion force of water droplets on microstructured hydrophobic surfaces," *Sensors and Actuators B: Chemical*, vol. 213, pp. 360–367, 2015.
- [55] Y. Zheng, X. Gao, and L. Jiang, "Directional adhesion of superhydrophobic butterfly wings," *Soft Matter*, vol. 3, no. 2, p. 178, 2007.

- [56] J. Zhang *et al.*, "Ratchet-induced anisotropic behavior of superparamagnetic microdroplet," *Applied Physics Letters*, vol. 94, no. 14, pp. 2007–2010, 2009.
- [57] M. Jin *et al.*, "Superhydrophobic aligned polystyrene nanotube films with high adhesive force," *Advanced Materials*, vol. 17, no. 16, pp. 1977–1981, 2005.
- [58] B. Samuel, H. Zhao, and K. Y. Law, "Study of wetting and adhesion interactions between water and various polymer and superhydrophobic surfaces," *Journal of Physical Chemistry C*, vol. 115, no. 30, pp. 14 852–14 861, 2011.
- [59] P. Roach, N. J. Shirtcliffe, and M. I. Newton, "Progress in superhydrophobic surface development," *Soft Matter*, vol. 4, p. 224, 2008.
- [60] Y. Y. Yan, N. Gao, and W. Barthlott, "Mimicking natural superhydrophobic surfaces and grasping the wetting process: a review on recent progress in preparing superhydrophobic surfaces." *Advances in colloid and interface science*, vol. 169, no. 2, pp. 80–105, Dec. 2011.
- [61] Y.-L. Zhang *et al.*, "Recent developments in superhydrophobic surfaces with unique structural and functional properties," *Soft Matter*, vol. 8, no. 44, p. 11217, 2012.
- [62] S. S. Latthe *et al.*, "Recent progress in preparation of superhydrophobic surfaces: a review," *Journal of Surface Engineered Materials and Advanced Technology*, vol. 2, pp. 76–94, 2012.
- [63] T. Darmanin and F. Guittard, "Recent Advances in the Potential Applications of Bioinspired Superhydrophobic Materials," *The Royal Society of Chemistry*, vol. 00, pp. 1–3, 2013.
- [64] H. Zhu, Z. Guo, and W. Liu, "Adhesion behaviors on superhydrophobic surfaces." *Chemical communications (Cambridge, England)*, vol. 50, no. 30, pp. 3900–13, 2014.
- [65] Y. Yoon, D. Kim, and J.-B. Lee, "Hierarchical micro/nano structures for superhydrophobic surfaces and super-lyophobic surface against liquid metal," *Micro Nano Syst. Lett.*, vol. 2, no. 1, p. 3, 2014.



- [66] B. N. Sahoo and B. Kandasubramanian, "Recent progress in fabrication and characterisation of hierarchical biomimetic superhydrophobic structures," *RSC Adv.*, vol. 4, no. 42, p. 22053, 2014.
- [67] P. Zhang and F. Lv, "A review of the recent advances in superhydrophobic surfaces and the emerging energy-related applications," *Energy*, vol. 82, pp. 1068–1087, 2015.
- [68] X. Zhang *et al.*, "Morphology and wettability control of silicon cone arrays using colloidal lithography," *Langmuir*, vol. 25, no. 13, pp. 7375–7382, 2009.
- [69] J. Park *et al.*, "Design and fabrication of a superhydrophobic glass surface with micro-network of nanopillars," *Journal of Colloid and Interface Science*, vol. 360, no. 1, pp. 272–279, 2011.
- [70] M. Sun *et al.*, "Artificial lotus leaf by nanocasting," *Langmuir*, vol. 21, no. 19, pp. 8978–8981, 2005.
- [71] D. E. Weibel *et al.*, "Adjustable hydrophobicity of Al substrates by chemical surface functionalization of nano/microstructures," *Journal of Physical Chemistry C*, vol. 114, no. 31, pp. 13 219–13 225, 2010.
- [72] P. Guo *et al.*, "Icephobic/anti-icing properties of micro/nanostructured surfaces." *Adv. Mater.*, vol. 24, no. 19, pp. 2642–8, 2012.
- [73] S. A. Kulinich *et al.*, "Superhydrophobic surfaces: Are they really ice-repellent?" *Langmuir*, vol. 27, pp. 25–29, 2011.
- [74] M. Nosonovsky and V. Hejazi, "Why superhydrophobic surfaces are not always icephobic." *ACS Nano*, vol. 6, no. 10, pp. 8488–91, 2012.
- [75] V. Hejazi, K. Sobolev, and M. Nosonovsky, "From superhydrophobicity to ice-phobicity: forces and interaction analysis." *Sci. Rep.*, vol. 3, p. 2194, 2013.
- [76] H. Liu, J. Zhai, and L. Jiang, "Wetting and anti-wetting on aligned carbon nanotube films," *Soft Matter*, vol. 2, no. 10, p. 811, 2006.
- [77] L.-Y. Meng and S.-J. Park, "Superhydrophobic carbon-based materials: a review of synthesis, structure, and applications," *Carbon Lett.*, vol. 15, no. 2, pp. 89–104, 2014.

- [78] Y. Liu *et al.*, "Artificial lotus leaf structures from assembling carbon nanotubes and their applications in hydrophobic textiles," *J. Mater. Chem.*, vol. 17, no. 11, p. 1071, 2007.
- [79] S. Sethi *et al.*, "Gecko-inspired carbon nanotube-based self-cleaning adhesives." *Nano Lett.*, vol. 8, no. 3, pp. 822–5, 2008.
- [80] Y. C. Hong and H. S. Uhm, "Superhydrophobicity of a material made from multiwalled carbon nanotubes," *Appl. Phys. Lett.*, vol. 88, no. 24, p. 244101, 2006.
- [81] F. D. Nicola *et al.*, "Super-hydrophobic multi-walled carbon nanotube coatings for stainless steel," *Nanotechnology*, vol. 26, no. 14, p. 145701, 2015.
- [82] L. Zhu *et al.*, "Superhydrophobicity on two-tier rough surfaces fabricated by controlled growth of aligned carbon nanotube arrays coated with fluorocarbon," *Langmuir*, no. 20, pp. 11 208–11 212, 2005.
- [83] B. Kakade and V. K. Pillai, "Tuning the wetting properties of multiwalled carbon nanotubes by surface functionalization," *The Journal of Physical Chemistry C*, vol. 112, no. 9, pp. 3183–3186, 2008.
- [84] C. Luo *et al.*, "Flexible carbon nanotube-polymer composite films with high conductivity and superhydrophobicity made by solution process," *Nano Lett.*, vol. 8, no. 12, pp. 4454–4458, 2008.
- [85] Y. Jung and B. Bhushan, "Mechanically durable carbon nanotube-composite hierarchical structures with superhydrophobicity, self-cleaning, and low-drag," *ACS Nano*, vol. 3, no. 12, pp. 4155–4163, 2009.
- [86] C.-H. Chen *et al.*, "Dropwise condensation on superhydrophobic surfaces with two-tier roughness," *Appl. Phys. Lett.*, vol. 90, no. 17, 2007.
- [87] J. Zou *et al.*, "Preparation of a Superhydrophobic and Conductive Nanocomposite Coating from a Carbon-Nanotube-Conjugated Block Copolymer Dispersion," *Adv. Mater.*, vol. 20, no. 17, pp. 3337–3341, 2008.
- [88] S. Sethi and A. Dhinojwala, "Superhydrophobic conductive carbon nanotube coatings for steel." *Langmuir*, vol. 25, no. 8, pp. 4311–3, 2009.

- [89] I. S. Bayer, A. Steele, and E. Loth, "Superhydrophobic and electroconductive carbon nanotube-fluorinated acrylic copolymer nanocomposites from emulsions," *Chem. Eng. J.*, vol. 221, pp. 522–530, 2013.
- [90] T. N. Krupenkin, J. A. Taylor, and E. N. Wang, "Reversible wetting-dewetting transitions on electrically tunable superhydrophobic nanostructured surfaces," *Langmuir*, vol. 23, no. 18, pp. 9128–9133, 2007.
- [91] A. Ahuja, J. A. Taylor, and V. Lifton, "Nanonails: A simple geometrical approach to electrically tunable superhydrophobic surfaces," *Langmuir*, vol. 24, no. 1, pp. 9–14, 2008.
- [92] S. Iijima, "Helical microtubules of graphitic carbon," *Nature*, 1991.
- [93] K. Teo and C. Singh, "Catalytic synthesis of carbon nanotubes and nanofibers," ...*of Nanoscience and ...*, vol. X, pp. 1–22, 2003.
- [94] C. Dupas and M. Lahmani, *Nanoscience: Nanotechnologies and nanophysics*. Springer, 2007.
- [95] S. Bellucci, "Carbon nanotubes: physics and applications," *Phys. Status Solidi*, vol. 2, no. 1, pp. 34–47, 2005.
- [96] M. Paradise and T. Goswami, "Carbon nanotubes – Production and industrial applications," *Materials & Design*, vol. 28, no. 5, pp. 1477–1489, Jan. 2007.
- [97] S. B. Sinnott and R. Andrews, "Carbon Nanotubes: Synthesis, Properties, and Applications," *Crit. Rev. Solid State Mater. Sci.*, vol. 26, no. 3, pp. 145–249, Jul. 2001.
- [98] A. Thess, R. Lee, and P. Nikolaev, "Crystalline ropes of metallic carbon nanotubes," ...*AAAS-Weekly Pap. ...*, no. July, pp. 483–487, 1996.
- [99] M. S. Bell *et al.*, "Carbon nanotubes by plasma-enhanced chemical vapor deposition," *Pure Appl. Chem.*, vol. 78, no. 6, pp. 1117–1125, 2006.
- [100] M. Meyyappan *et al.*, "Carbon nanotube growth by PECVD: a review," *Plasma Sources Sci. Technol.*, vol. 12, no. 2, pp. 205–216, 2003.

- [101] M. Quirk and J. Serda, *Semiconductor Manufacturing Technology*. Prentice Hall, 2000.
- [102] C. Bower *et al.*, "Plasma-induced alignment of carbon nanotubes," *Applied Physics Letters*, vol. 77, no. 6, p. 830, 2000.
- [103] K. B. K. Teo *et al.*, "Characterization of plasma-enhanced chemical vapor deposition carbon nanotubes by Auger electron spectroscopy," *J. Vac. Sci. Technol. B Microelectron. Nanom. Struct.*, vol. 20, no. 1, p. 116, 2002.
- [104] M. Chhowalla *et al.*, "Growth process conditions of vertically aligned carbon nanotubes using plasma enhanced chemical vapor deposition," *J. Appl. Phys.*, vol. 90, no. 10, p. 5308, 2001.
- [105] Y. J. Jung *et al.*, "Mechanism of Selective Growth of Carbon Nanotubes on SiO<sub>2</sub>/Si Patterns," *Nano letters*, vol. 3, no. 4, pp. 2–5, 2003.
- [106] a. V. Melechko *et al.*, "Vertically aligned carbon nanofibers and related structures: Controlled synthesis and directed assembly," *Journal of Applied Physics*, vol. 97, no. 4, p. 041301, 2005.
- [107] C.-M. Seah, S.-P. Chai, and A. R. Mohamed, "Synthesis of aligned carbon nanotubes," *Carbon*, vol. 49, no. 14, pp. 4613–4635, 2011.
- [108] R. M. Silva *et al.*, "Ultra simple catalyst layer preparation for the growth of vertically aligned CNTs and CNT-based nanostructures," *CrystEngComm*, vol. 14, p. 48, 2012.
- [109] A. Jorio, G. Dresselhaus, and M. Dresselhaus, *Carbon nanotubes: advanced topics in the synthesis, structure, properties and applications*. Springer, 2007.
- [110] V. M. Sivakumar *et al.*, "Optimized parameters for carbon nanotubes synthesis over Fe and Ni catalysts VIA methane CVD," *Reviews on Advanced Materials Science*, vol. 27, no. 1, pp. 25–30, 2011.
- [111] D. Park, Y. H. Kim, and J. K. Lee, "Pretreatment of stainless steel substrate surface for the growth of carbon nanotubes by PECVD," *Journal of Materials Science*, vol. 38, no. 24, pp. 4933–4939, Dec. 2003.

- [112] R. Baker, "Catalytic growth of carbon filaments," *Carbon*, vol. 27, no. 3, pp. 315–323, 1989.
- [113] a. Gohier *et al.*, "Carbon nanotube growth mechanism switches from tip- to base-growth with decreasing catalyst particle size," *Carbon*, vol. 46, no. 10, pp. 1331–1338, 2008.
- [114] K. E. Nordheim, "Growth and properties of Carbon Nanotubes," Master Thesis, The Norwegian University of Science and Technology, 2012.
- [115] Ø. Våland, "Innovative Utilization of Carbon Nanotubes in Marine and Off-shore Oil/Gas Applications," Master Thesis, The Norwegian University of Science and Technology, 2013.
- [116] NTNU Nanolab, "Dynatex DX-III Scriber Tool Description," <http://ntnu.norfab.no/WebForms/Equipment/EquipmentView.aspx?toolId=42>, [Online; accessed 20-June-2015].
- [117] NTNU Nanolab, "Diener Electronics Femto Plasma Cleaner Tool Description," <http://ntnu.norfab.no/WebForms/Equipment/EquipmentView.aspx?toolId=38>, [Online; accessed 20-June-2015].
- [118] C. Mattevi, C. Wirth, and S. Hofmann, "In-situ X-ray photoelectron spectroscopy study of catalyst - support interactions and growth of carbon nanotube forests," *J. Phys. Chem. C*, vol. 112, pp. 12 207–12 213, 2008.
- [119] NTNU Nanolab, "AJA International Inc. Custom ATC-2200B AJA Sputter and Evaporator Tool Description," <http://ntnu.norfab.no/WebForms/Equipment/EquipmentView.aspx?toolId=73>, [Online; accessed 20-June-2015].
- [120] NTNU Nanolab, "Oxford Instruments PlasmaLab System 100-PECVD Tool Description," <http://ntnu.norfab.no/WebForms/Equipment/EquipmentView.aspx?toolId=33>, [Online; accessed 20-June-2015].
- [121] T. Xu *et al.*, "Surface modification of multi-walled carbon nanotubes by O<sub>2</sub> plasma," *Applied Surface Science*, vol. 253, no. 22, pp. 8945–8951, 2007.

- [122] B. Zhao *et al.*, "Surface functionalization of vertically-aligned carbon nanotube forests by radio-frequency Ar/O<sub>2</sub> plasma," *Carbon*, vol. 50, no. 8, pp. 2710–2716, 2012.
- [123] P. Mishra, Harsh, and S. S. Islam, "Surface modification of MWCNTs by O<sub>2</sub> plasma treatment and its exposure time dependent analysis by SEM, TEM and vibrational spectroscopy," *Superlattices and Microstructures*, vol. 64, pp. 399–407, 2013.
- [124] J. Feng *et al.*, "Why condensate drops can spontaneously move away on some superhydrophobic surfaces but not on others," *ACS Applied Materials and Interfaces*, vol. 4, no. 12, pp. 6618–6625, 2012.
- [125] NTNU Nanolab, "Hitachi S-5500 S(T)EM Key Product Features," [http://www.jeolusa.com/PRODUCTS/TransmissionElectronMicroscopes\(TEM\)/200kV/JEM-2100F/tabid/208/Default.aspx](http://www.jeolusa.com/PRODUCTS/TransmissionElectronMicroscopes(TEM)/200kV/JEM-2100F/tabid/208/Default.aspx), [Online; accessed 20-June-2015].
- [126] NTNU Nanolab, "JEOL JEM-2100F TEM," <http://ntnu.norfab.no/WebForms/Equipment/EquipmentView.aspx?toolId=11>, [Online; accessed 20-June-2015].
- [127] DataPhysics Instruments GmbH, "DCAT 11 - Dynamic Contact Angle Measuring Instrument and Tensiometer," [http://www.dataphysics.de/?cat\\_id=95&lang=EN](http://www.dataphysics.de/?cat_id=95&lang=EN), [Online; accessed 20-June-2015].

# Appendices





# Appendix A

## TEM Results

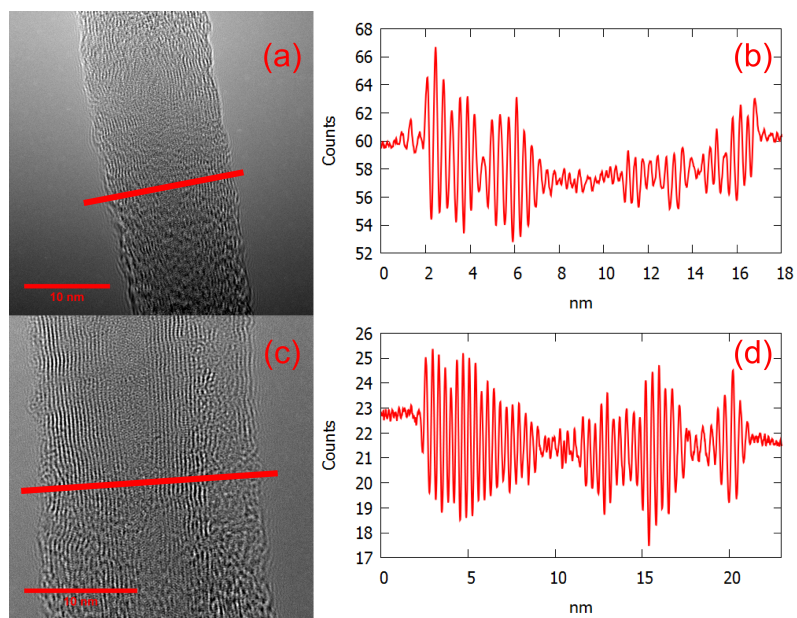


**Figure A.1:** The carbon nanotube wall structure from figures 5.2(a)–(b) were analysed by the counting of wall planes along the red line.

The transmission electron microscope images from figure 5.2(a)–(b) are more closely investigated in figure A.1 by the use of a colour-intensity counter. This method scans the tube perpendicular to its axis, allowing the number of tube walls to be counted, and the interatomic distance between them to be determined.

# Appendix B

## Water Adhesion Results

Figure B.1 includes the adhesive force curves of all surfaces tested in this thesis. The values for maximum force and snap-in force summarised in table 5.1 are extracted from the curves from the points indicated in figure 5.7. Notice that the force curve of surface 5 is nearly identical to 6 and might be hard to see.

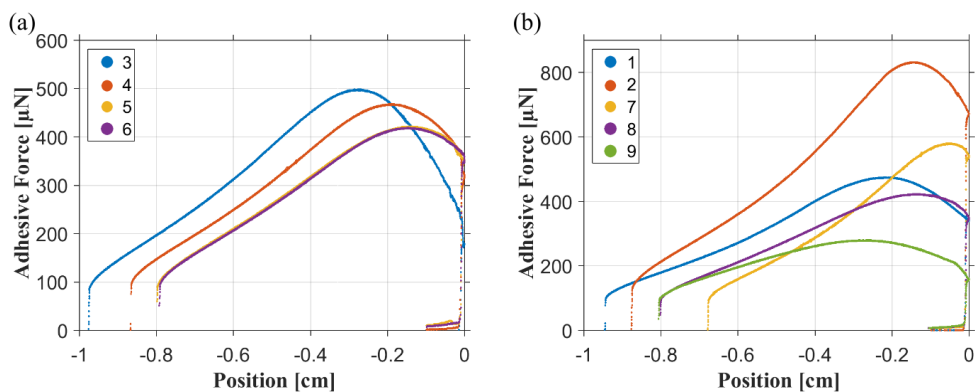


**Figure B.1:** Adhesive force measurements of the surfaces listed in table 5.1. The samples with differing FDTS immersion times are shown in (a), while the remaining samples are in (b).